energies

MDPI

Article

Simultaneous Optimization of Network Reconfiguration and Soft Open Points Placement in Radial Distribution Systems Using a Lévy Flight-Based Improved Equilibrium Optimizer

Ridha Djamel Mohammedi [1], Djamal Gozim [2], Abdellah Kouzou [1,*], Mustafa Mosbah [3], Ahmed Hafaifa [1], Jose Rodriguez [4] and Mohamed Abdelrahem [5,6,*]

[1] Laboratory of Applied Automation and Industrial Diagnostics (LAADI), Faculty of Sciences and Technology, Ziane Achour University of Djelfa, Djelfa 17000, Algeria; r.mohammedi@univ-djelfa.dz (R.D.M.); a.hafaifa@univ-djelfa.dz (A.H.)
[2] Department of Electrical Engineering, Ziane Achour University of Djelfa, Djelfa 17000, Algeria; d.gozim@univ-djelfa.dz
[3] Faculty of Science and Technology, Université de Ghardaia, Ghardaia 47000, Algeria; m.mosbah@lagh-univ.dz
[4] Director Center for Energy Transition, Universidad San Sebastián, Santiago 8420524, Chile; jose.rodriguezp@uss.cl
[5] Department of Electrical Engineering, Faculty of Engineering, Assiut University, Assiut 71516, Egypt
[6] Chair of High-Power Converter Systems, Technical University of Munich, 80333 Munich, Germany
* Correspondence: a.kouzou@univ-djelfa.dz (A.K.); mohamed.abdelrahem@tum.de (M.A.)

Abstract: This research paper focuses on the application of a new method for the simultaneous reconfiguration and the optimum placing of Soft Open Points (SOPs) in Radial Distribution Systems (RDS). The proposed Lévy Flight-based Improved Equilibrium Optimizer (LF-IEO) algorithm enhances the standard Equilibrium Optimizer (EO) by integrating several techniques to improve exploration and exploitation capabilities. SOPs are highly developed power electronics devices that can enhance distribution utility networks in terms of reliability and effectiveness. However, identifying their optimum place along with network reconfiguration is a challenging task that requires advanced computation techniques. The performance of the proposed LF-IEO algorithm has been first verified on several benchmark functions. Subsequently, it is implemented on a IEEE 33-Bus, 69-Bus, 118-Bus, and Algerian 116-Bus distribution network to solve the problem of simultaneous network reconfiguration and optimal SOP placement. For the Algerian 116-bus system case study, the algorithm achieved a significant 14.89% reduction in power losses, improved the minimum voltage, and generated substantial net annual savings of 74,426.40 $/year. To prove its superiority in terms of solution quality and robustness, the proposed LF-IEO approach was compared with several newly developed algorithms from the literature.

Keywords: soft open points; radial distribution systems; lévy flight-based improved equilibrium optimizer; network reconfiguration; voltage profile; power loss reduction; optimization

Citation: Mohammedi, R.D.; Gozim, D.; Kouzou, A.; Mosbah, M.; Hafaifa, A.; Rodriguez, J.; Abdelrahem, M. Simultaneous Optimization of Network Reconfiguration and Soft Open Points Placement in Radial Distribution Systems Using a Lévy Flight-Based Improved Equilibrium Optimizer. *Energies* **2024**, *17*, 5911. https://doi.org/10.3390/en17235911

Academic Editor: Ahmed Abu-Siada

Received: 8 September 2024
Revised: 18 November 2024
Accepted: 22 November 2024
Published: 25 November 2024

1. Introduction

Electrical distribution systems are the last link in the power delivery chain and typically operate radially to provide protection and maintain low fault currents. However, these systems face several challenges, the most significant being active power losses that can reach up to 20% of the total power [1]. It is crucial to address these losses to improve the efficiency and reliability of the system. Several solutions have been proposed, including shunt compensators, network reconfiguration, and Flexible AC Transmission Systems (FACTS; see Appendix A for the List of Abbreviations). In addition to these classical mitigations, a new and indeed promising one presumes simultaneous arrangement of Soft Open Points (SOPs) along with network reconfiguration. Nevertheless, a robust

optimization strategy is required, as any incorrectly arranged configuration may cause a negative impact on the system.

Distribution System Reconfiguration (DSR) is a method to optimize Radial Distribution Systems (RDS) by altering the network topology through switching actions. This process rearranges the network topology to create a radial structure that meets specific objectives, such as minimizing losses and improving voltage profiles. However, DSR is considered a complex problem in mathematics and is classified as a mixed-integer non-linear problem [2]. Its complexity arises from two main challenges: first, solving power flow equations while considering the discrete nature of switch operations; second, determining the optimal status of switches to achieve the best possible reconfiguration.

SOPs represent an advanced power electronic device, and they find a useful application within distribution systems [3]. As shown in Figure 1, SOPs provide significant improvements in the reconfiguration and operation of RDS over conventional tie switches. The key difference between the two is that the SOP can bidirectionally control the flow of active and reactive power between the feeders, while a tie switch only acts as an on/off switch. Figure 1a illustrates a simple configuration of a distribution system with SOP, while Figure 1b shows the core circuit topology of the VSC-based SOP. This enhanced controllability places SOPs in a position to achieve optimal voltage levels across the network for minimum loss of power through intelligent management and optimal distribution of power transfer between feeders. When used in combination with other network equipment, SOPs allow system operators to carry out network changes much more quickly and efficiently, with a much wider range of flexible configurations. Tie switches, on the other hand, can only permit improvements at a much slower rate. The introduction of SOPs helps in making responsive modifications, at relatively shorter intervals, to the changes in load patterns and significantly improves the overall performance of the system.

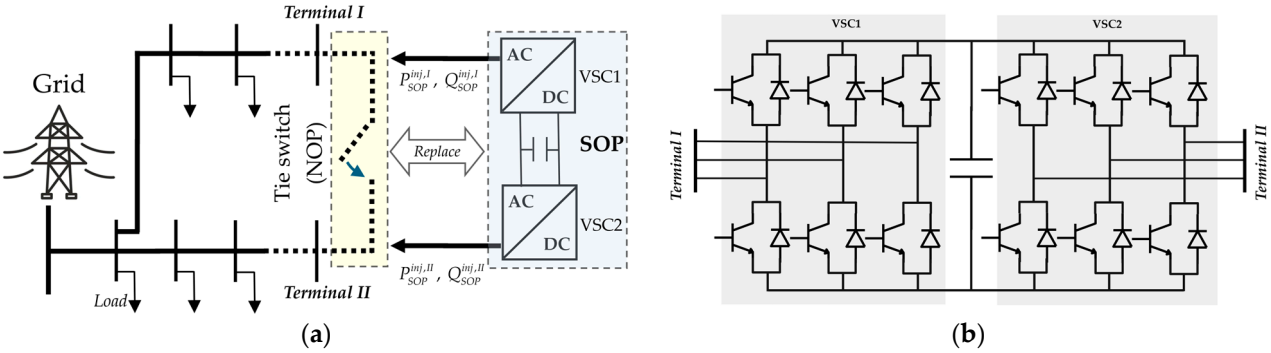

Figure 1. (**a**) Simple configuration of a distribution system with SOP; (**b**) Core circuit design of the VSC-based SOP.

Recently, numerous algorithms have been developed for the optimal placement and sizing of SOPs in RDS. These algorithms mainly use metaheuristic techniques, which are well known for their ability to find global solutions, avoid local minimum traps, and effectively explore vast solution spaces. Examples include Particle Swarm Optimization (PSO) [4], which simulates the social behavior of fish and birds; Artificial Rabbits Optimization (ARO) [5], inspired by the searching behavior of rabbits; Political Optimizer (PO) [6], which mimics political negotiations; Mixed-Integer Second-Order Cone Programming (MISOCP) [7], a mathematical method for non-linear optimization; Stackelberg Game (SG) [8], based on leader-follower dynamics; Modified Grey Wolf Optimization (MGWO) [9], which adapts the hunting strategies of grey wolves; Hybrid Simulated Annealing with Second-Order Cone Programming (Hybrid SA-SOCP) [10], combining probabilistic search with cone programming; Multi-Objective Particle Swarm Optimization (MOPSO) [11,12], a variant of PSO for multiple objectives; Genetic Algorithm (GA) [13], which uses evolutionary principles; Artificial Bee Colony (ABC) [14], modeled after the foraging behavior of bees; Growth Optimizer (GO) [15], which simulates natural growth;

Differential Evolution (DE) [16], a population-based algorithm; Adaptive Alternating Direction Method of Multipliers (ADMM) [17], for large-scale optimization; Hyper-Spherical Discrete-Continuous Search (HS-DCS) [18], which explores high-dimensional spaces; Improved Powell's Direct Set (IPDS) [19], an enhanced derivative-free technique; and Tunicate Swarm Algorithm (TSA) [20], inspired by marine organisms. One noticeable trend is that most of the recent research does not consider both the placement and reconfiguration of SOPs simultaneously. In fact, a review of the latest studies shows that less than 10% address both elements. Additionally, most recent research primarily focuses on minimizing power loss in the system. However, these studies often neglect to account for the installation and maintenance costs of SOPs, as well as the power losses occurring within these devices themselves.

This study introduces a novel Lévy Flight-based Improved Equilibrium Optimizer (LF-IEO) algorithm for the simultaneous optimization of network reconfiguration and SOPs placement in radial distribution systems. The LF-IEO algorithm incorporates several key enhancements to address the limitations of the conventional Equilibrium Optimizer (EO). These include a Good Point Set (GPS) initialization technique to improve initial population diversity, a Lévy Flight strategy to enhance exploration capabilities, Fast Random Opposition-Based Learning (FROBL) to accelerate convergence, and an Oscillating Generation Probability (OGP) to balance exploration and exploitation strategies.

The major contributions of the present paper are:

- Proposing a new method for optimal reconfiguration of RDS, including SOPs based on graph theory.
- Introducing the Lévy Flight-based Improved Equilibrium Optimizer (LF-IEO) algorithm for solving the optimization problem. This algorithm incorporates several enhancements to improve performance and convergence.
- Applying the proposed method to test networks, including the IEEE 33-bus, IEEE 69-bus, and IEEE 118-bus systems, and validating it on an Algerian power company's 116-bus distribution system, demonstrating its scalability and real-world applicability.

Following this introduction, the remainder of the paper is organized as follows: Section 2 discusses the methodology, detailing the LF-IEO algorithm and its enhancements. Section 3 presents the problem formulation, including SOPs modeling, objective function, and system constraints. Section 4 describes the application of LF-IEO to the proposed problem, including encoding/decoding solutions and the algorithm's flowchart. Section 5 presents the simulation results and discussion, analyzing the performance of LF-IEO on various test systems and comparing it with other algorithms. Finally, conclusions are given in Section 6.

2. Methodology

2.1. Equilibrium Optimizer (EO)

In 2020, Faramarzi et al. introduced the Equilibrium Optimizer (EO) as a new robust metaheuristic optimization algorithm [21]. This algorithm attempts to achieve dynamic equilibrium by balancing the mass in a control volume, mimicking the physical process. Like other population-based optimization methods, the candidate solutions are adapted based on the simulation of these states, guided by physical principles. A fitness function will have to balance between exploration and exploitation, driving the search space toward optimal solutions. The EO has several advantages, including simplicity, being parameter-free, derivative-free, and having a strong theoretical foundation and a comprehensive conceptual framework.

As with other metaheuristic algorithms, EO begins by randomly initializing a population of particles within the search space. Mathematically:

$$X^{initial} = LOB + rand(n, d) \times (UPB - LOB) \quad (1)$$

where $X^{initial}$ corresponds to the initial positions of the particles, LOB to the lower bound of the search space, and UPB to the upper bound. $rand(n, d)$ is used to generate a matrix of random numbers between 0 and 1, with dimensions $n \times d$, where n represents the number of particles and d represents the number of dimensions.

Each particle's fitness is calculated by the objective function, which is problem-dependent; the equilibrium pool contains the best individuals, forming a guide into the search process carried on by the entire population. The equilibrium pool comprises the five members:

$$E_{pool}^{itr} = \left\{ E_1^{itr}, E_2^{itr}, E_3^{itr}, E_4^{itr}, E_5^{itr} \right\} \tag{2}$$

where E_1^{itr} through E_4^{itr} represent the four best solutions found in the current iteration itr. The fifth member, E_5^{itr}, is the arithmetic mean of the other four, calculated by averaging their positions in the search space.

Particles update their concentrations (positions) towards the equilibrium state based on a randomly selected equilibrium candidate E_i from the equilibrium pool as follows:

$$X^{itr+1} = E_i + (X^{itr} - E_i)F + \frac{G}{\lambda V}(1 - F) \tag{3}$$

where X^{itr} represents the particle concentration (position) at the current iteration itr, F is an exponential term controlling the balance between exploration and exploitation, G is the generation rate for exploitation, λ is the turnover rate, and V is a constant unit volume. The exponential term F is calculated as:

$$\begin{cases} F = a_1 \times sign(r - 0.5)\left(e^{-\lambda t} - 1\right) \\ t = (1 - itr/itr_{\max})^{a_2(itr/itr_{\max})} \end{cases} \tag{4}$$

where a_1 and a_2 are constant coefficients that control the algorithm's exploration and exploitation capabilities. r is a random number between 0 and 1, itr represents the current iteration number, $itr_{\max}$ represents the maximum number of iterations, and λ represents the turnover rate. The generation rate G can be expressed as follows:

$$G = \begin{cases} -0.5 r_1 \left(E_i - \lambda X^{itr}\right) F, & \text{if } r_2 \geq GP \\ 0, & \text{if } r_2 < GP \end{cases} \tag{5}$$

where r_1, r_2 are random numbers between 0 and 1, λ is a control parameter, and GP is the generation control parameter usually taken as 0.5. Equations (2) through (5) work together to guide the particles towards optimal solutions, balancing exploration of the search space with exploitation of promising areas. The steps of the EO algorithm are presented in Algorithm 1.

Since its introduction, EO has emerged as a promising metaheuristic technique for addressing a variety of power system challenges. EO was used by Mansour et al. [22] to improve the performance of automatic generation control (AGC) against renewable energy disturbances. Zellagui et al. [23] used EO to determine the optimal location of photovoltaic distributed generators in medium-voltage DC networks, considering both technical and economic factors. In [24], Mohammedi et al. utilized EO to coordinate overcurrent relays, ensuring fault protection. Korashy et al. [25] proposed an improved EO algorithm that shows superior performance over traditional methods to coordinate directional overcurrent and distance relays. For solving temperature-dependent optimal power flow problems, Dao et al. [26] introduced a chaotic EO variant, demonstrating its efficacy across different objective functions. In grid-tied PV systems, Chankaya et al. [27] applied EO to enhance power quality and system dynamics.

Algorithm 1: Equilibrium Optimizer (EO)

Input: n (Population size), d (dimension of the search space), LOB (Lower Bound of search space), UPB (Upper Bound of search space), itr_{max} (Maximum number of iterations)

Output: X^* (The best solution found)

Initialize the population randomly using the Equation (1)
Evaluate the fitness of each particle
for $itr = 1$ *to* itr_{max} **do**
    Select top candidates to form the equilibrium pool E_{pool}^{itr} defined in Equation (2)
    for $i = 1$ *to* n **do**
        Select a random equilibrium candidate E_i from E_{pool}^{itr}
        Calculate F using Equation (4)
        Calculate G using Equation (5)
        Update particle position using Equation (3)
    end
    Evaluate the fitness of each particle and update E_{pool}^{itr}
end
Return The best solution from E_{pool}^{itr}

As a result of these diverse applications, EO has shown its versatility and effectiveness in addressing a wide range of optimization challenges across many different aspects of power system operation and control.

2.2. The Proposed Levy Flight-Based Improved Equilibrium Optimizer (LF-IEO)

This paper presents the LF-IEO as an improvement of the standard EO. Although the EO presents a high convergence and good precision, it exhibits poor exploration capability, unbalanced exploration-exploitation capabilities, a tendency to get entrapped into local optima, and suboptimal initialization population creation. To overcome these limitations, LF-IEO integrates several important improvements in the basic EO framework. These improvements include an enhanced initialization technique, a better search strategy, a modified learning approach, and dynamic parameter adjustment. The LF-IEO, through these changes, tries to increase the exploration and exploitation power of the parent algorithm so that better and more reliable optimization results can be achieved in wide areas of application.

A. Good Point Set-based (GPS) initialization

The initialization of the population significantly influences the performance of metaheuristic optimization algorithms. A well-distributed initial population might enhance diversity, help speed up the convergence process, and thus prevent premature convergence to local optima. The usual EO algorithm employs random initialization with a lack of intelligence in the distribution of solutions. The initialization of such a solution set might, by chance, locate all solutions close to some of the optima while disregarding other promising regions of the search space. This uneven coverage is prone to ineffective searching and suboptimal performance. Consequently, a uniformly distributed initial population has to be ensured. The GPS initialization process offers an efficient way to achieve a more uniformly dispersed initial population [28]. This procedure is based on number theory concepts and generates low-discrepancy points that achieve much better coverage of the search

space than random initialization. Therefore, to enrich the exploration and convergence capacities of the EO algorithm, GPS-based initialization is incorporated in the proposed LF-IEO variant. This initialization strategy gives a variety and an even distribution in the initial population, which will help in providing the base for further search processes. Algorithm 2: Describe the GPS-based steps. Figure 2 compares population initialization methods in two dimensions: (a) the standard random approach and (b) the GPS technique. The GPS-based initialization technique gives rise to a more uniform population distribution and a higher-quality population.

Algorithm 2: GPS-based Initialization

Input: n (Population size), n (dimension of the search space), LOB (Lower Bound of search space), UPB (Upper Bound of search space)

Output: Population (Initial population)

Find the minimum prime number ρ such that $\rho \geq 2\,n + 3$
for $j = 1$ *to* n **do**
  $r(j) = 2 \times cos(2\pi \times j \,/\, \rho)$
end
for $i = 1$ *to* n **do**
  for $j = 1$ *to* d **do**
    $Population\,[i, j] = LOB[j] + mod(r(j) \times i, 1) \times (UPB[j] - LOB[j])$
  end
end
Return Population

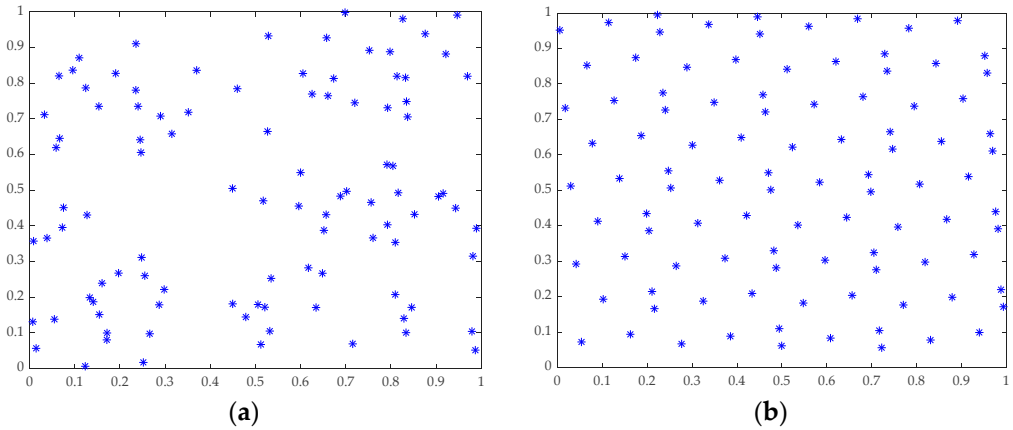

Figure 2. Comparison of population initialization methods in two dimensions: (**a**) Standard random approach; (**b**) GPS technique.

B. Levy Flight (LF) strategy

Lévy flight is a category of random walk behavior in which large jumps occur infrequently and lead to significant performance enhancement for algorithms in the domain of metaheuristics [29]. This distinctive movement strategy is inspired by the foraging patterns of various animals in nature and provides an effective mechanism for balancing exploration and exploitation in optimization problems. In the framework of global optimization, the heavy-tailed distribution of Lévy flight allows algorithms to escape local optima more efficiently than traditional random walk methods. The diversification capability of the

LF-IEO algorithm is greatly enhanced by incorporating Lévy flight, thereby preserving population diversity over time. This attribute helps mitigate the common issue associated with metaheuristic techniques, such as premature convergence, observed in standard EO. With the integration of Lévy flight, the search pattern consistently combines frequent small-scale movements with occasional large jumps, broadening the exploration space and thereby increasing the algorithm's potential to efficiently locate optimal regions in the search landscape.

The Lévy flight strategy can be mathematically written in the following form and integrated into the LF-IEO algorithm:

$$Levy = \left(0.01 \times \mu / |v|^{1/\beta}\right) \tag{6}$$

where: $\mu \sim N(0, \sigma_\mu^2)$, and $v \sim N(0, \sigma_v^2)$, are drawn from normal distributions, and β is a parameter between 1 and 2, typically set to 1.5.

$$\sigma_\mu = \left\{ \frac{\Gamma(1+\beta) \times \sin(\pi\beta/2)}{\Gamma(0.5+\beta/2) \times \beta \times 2^{\beta/2-0.5}} \right\}^{1/\beta}, \ \sigma_v = 1 \tag{7}$$

where σ_μ represents the standard deviation of the distribution for μ, while σ_v is set to 1.

Next, the new position of a search agent is calculated by applying:

$$X' = X + rand_1(d, 1) \times sign(rand_2 - 0.5) \times Levy \times (X - X_{TARGET}) \tag{8}$$

where $rand_{1,2}$ are random numbers between 0 and 1, $sign(\cdot)$ is the sign function, and X_{TARGET} is the target position (best-known solution). The movement is made to perform both small local displacements and occasional large jumps in the solution space, which gives this form of formulation advantages in efficiently exploring search space against being stuck at a single location (local minimum).

C. Fast Random Opposition-Based Learning FROBL

The FROBL technique is incorporated into the proposed LF-IEO algorithm to improve both exploration and exploitation capabilities. FROBL generates solutions that are opposite to the current population members, potentially discovering promising new regions of the search space. As shown in Algorithm 3, FROBL utilizes a modified formulation of the original opposition-based learning approach [30]. A sinusoidal function is introduced to create controlled randomness when calculating opposite solutions. The sine term $\sin(2\pi \times r)$ oscillates between -1 and 1, allowing the opposite solutions to be generated within a bounded region around the midpoint of the search space. This sinusoidal variation helps maintain diversity while still focusing the search near promising areas. The algorithm also introduces an adaptive factor k that decreases over iterations, gradually reducing the magnitude of changes to facilitate convergence. By balancing exploration early on and exploitation in later stages, FROBL aims to improve the algorithm's ability to avoid local optima and increase its convergence speed toward the global optimum.

Algorithm 3: Fast random opposition-based learning

Input: *Population* (Current population), *n* (Population size), *d* (dimension of the search space), *itr* (Current Iteration), itr_{max} (Maximum number of iterations), *LOB* (Lower Bound of search space), *UPB* (Upper Bound of search space)

Output: *Opposite* (Opposite population)

$k = \left(1 + \sqrt{itr / itr^{max}}\right)^{10}$

for *i = 1 to n* **do**

  for *j = 1 to d* **do**

    $r = random(0,1)$, $mid(j) = \left(UPB(j) - LOB(j)\right) / 2$

    if $Population\left[i,j\right] < mid(j)$ **then**

      $Opposite\left[i,j\right] = mid(j) + r^2 \times sin\left(2\pi \times r\right) \times Population\left[i,j\right] / 2k$

    else

      $Opposite\left[i,j\right] = mid(j) - r^2 \times sin\left(2\pi \times r\right) \times Population\left[i,j\right] / 2k$

    end

  end

end

Return *Opposite*

D. Enhancing EO with Oscillating Generation Probability.

An important update in LF-IEO is the dynamic adjustment of the Generation Probability (*GP* parameter). In the standard EO, it has been assigned a constant value of 0.5, whereas the LF-IEO uses a sinusoidal variation of *GP* defined as:

$$GP = 0.25\left(1 + \sin\left(2\pi \frac{itr}{itr_{\max}}\right)\right) \quad (9)$$

Such a sinusoidal formulation allows for a finer balance between exploration and exploitation throughout the optimization process. This approach allows the algorithm to switch between an intensive exploration and a focused exploitation phase during optimization, allowing for potentially highly extensive searches of the solution space and better convergence towards the global optima. This *GP* modification complements the other enhancements implemented in the LF-IEO, collectively addressing the limitations of the original EO and improving its overall optimization capabilities.

E. Key Advantages of LF-IEO

The proposed LF-IEO algorithm offers several distinct advantages over existing optimization techniques and variants of the EO method. These advantages can be summarized as follows:

- Enhanced Search Space Exploration:
  - The GPS initialization ensures a more uniform initial population distribution compared to random initialization, providing better coverage of the search space from the start.
  - The LF strategy allows both small-scale local searches and random big jumps, which allow the algorithm to break out of local optima faster than random walks.

- Improved Local Optima Avoidance:
  - The FROBL mechanism generates opposite solutions with controlled randomness through a sinusoidal function, helping avoid local optima traps. Additionally, an adaptive factor k in FROBL decreases over iterations, providing a natural transition from exploration to exploitation.
- Balanced Exploration-Exploitation:
  - The combination of the LF strategy and the FROBL mechanism provides an effective balance between global exploration and local exploitation. This adaptive balance helps avoid premature convergence while ensuring efficient convergence to optimal solutions.
- Computational Efficiency:
  - GPS initialization reduces the number of iterations needed to find high-quality solutions, thereby considerably reducing the computation time required to reach the optimal solution.

2.3. LF-IEO Performance Evaluation

To assess the performance of the proposed LF-IEO algorithm, eight benchmark functions commonly used in the literature were utilized: Sphere, Schwefel, Beale, Ackley, Rastrigin, Griewank, Shekel, and Penalized. The benchmark functions are divided into two categories: unimodal and multimodal. Functions F1 and F2 fall under the unimodal category, each possessing a single global optimum. The remaining functions, F3 through F8, are multimodal, featuring multiple local optima. These allow us to evaluate LF-IEO's ability to find the global optimum in more complex landscapes. Table 1 presents the mathematical formulations, dimensions, global optima, and search ranges for each of the selected benchmark functions. The performance of the proposed LF-IEO is compared with seven recently developed algorithms known for their effectiveness, namely the Grey Wolf Optimizer (GWO) [31], the Butterfly Optimization Algorithm (BOA) [32], the Whale Optimization Algorithm (WOA) [33], the Multi-Verse Optimizer (MVO) [34], the Salp Swarm Algorithm (SSA) [35], the Ant Lion Optimizer (ALO) [36], and the Sine Cosine Algorithm (SCA) [37], as well as the conventional EO. Moreover, Table 2 outlines the specific parameter configurations for all algorithms in the comparison. Each algorithm runs for a maximum of 60 iterations. To ensure statistical reliability, every algorithm was executed 30 independent times for each test function. Table 3 presents the results of these multiple runs, including the minimum, average, maximum, and standard deviation values. The optimization methods are then placed in order according to their average performance values. The average rank for all benchmark tests is also calculated to determine the overall ranking. All algorithms are implemented using MATLAB software installed on a PC with an Intel Core i9-14700K processor, a 5.60 GHz clock frequency, and 64 GB of memory on OS Windows 11.

Based on the results presented in Table 3 and the convergence curves shown in Figures 3–8, the Flight LF-IEO demonstrates superior performance compared to other algorithms across various benchmark functions. For the Sphere function (F1), LF-IEO consistently achieves the optimal solution with zero error, outperforming all other algorithms, including the original EO. The convergence curve in Figure 3b shows that LF-IEO converges rapidly to the global optimum, maintaining a significant lead over other algorithms throughout the optimization process. Similar superior performance is observed for the Schwefel function (F2), where LF-IEO again achieves zero error and exhibits the fastest convergence, as seen in Figure 3b. For the Beale function (F3), LF-IEO ranks second, very close to EO, but still outperforms other algorithms, with both showing rapid convergence in Figure 4b. In the case of the Ackley function (F4), LF-IEO once again achieves the best performance with zero error and the fastest convergence, as evident in Figure 5b. These results consistently demonstrate LF-IEO's enhanced ability to balance exploration and exploitation, allowing it to efficiently navigate complex search spaces and avoid local optima. The algorithm's performance is particularly impressive in both unimodal and

multimodal functions, indicating its versatility and robustness across different types of optimization problems.

Table 1. Benchmark functions.

Function	Mathematical Formulation	Range	n	x^*	$F(x^*)$
Sphere	$F_1(x) = \sum_{i=1}^{n} x_i^2$	$[-5.12,\ 5.12]$	30	$[0, \ldots, 0]$	0
Schwefel	$F_2(x) = \max\{\lvert x_i \rvert,\ 1 \le i \le n\}$	$[-100,\ 100]$	30	$[0, \ldots, 0]$	0
Beale	$F_3(x) = (x_1 x_2 + 1.5 - x_1)^2 + (x_1 x_2^2 + 2.25 - x_1)^2 + (x_1 x_2^3 + 2.625 - x_1)^2$	$[-4.5,\ 4.5]$	2	$[3, 0.5]$	0
Ackley	$F_4(x) = -20 \times \exp\left(-0.2\sqrt{\frac{1}{n}\sum_{i=1}^{n} x_i^2}\right) - \exp\left(\frac{1}{n}\sum_{i=1}^{n} \cos(2\pi x_i)\right) + e + 20$	$[-32.768,\ 32.768]$	30	$[0, \ldots, 0]$	0
Rastrigin	$F_5(x) = 10n + \sum_{i=1}^{n} \left[x_i^2 - 10\cos(2\pi x_i)\right]$	$[-5.12,\ 5.12]$	30	$[0, \ldots, 0]$	0
Griewank	$F_6(x) = \frac{1}{4000}\sum_{i=1}^{n} x_i^2 - \prod_{i=1}^{n} \cos\left(\frac{x_i}{\sqrt{i}}\right) + 1$	$[-600,\ 600]$	30	$[0, \ldots, 0]$	0
Shekel	$a = \begin{pmatrix} 4 & 1 & 8 & 6 & 3 & 2 & 5 & 8 & 6 & 7 \\ 4 & 1 & 8 & 6 & 7 & 9 & 5 & 1 & 2 & 3.6 \\ 4 & 1 & 8 & 6 & 3 & 2 & 3 & 8 & 6 & 7 \\ 4 & 1 & 8 & 6 & 7 & 9 & 3 & 1 & 2 & 3.6 \end{pmatrix}$ $c = \begin{pmatrix} 0.1 \\ 0.2 \\ 0.2 \\ 0.4 \\ 0.4 \\ 0.6 \\ 0.3 \\ 0.7 \\ 0.5 \\ 0.5 \end{pmatrix}$ $F_7 = -\sum_{i=1}^{10} \frac{1}{\sum_{j=1}^{4} (x_j - a_{ij})^2 + c_i}$	$[0,\ \pi]$	4	$[4, 4, 4, 4]$	-10.1532
Penalized	$F_8(x) = \left(\sum_{i=1}^{n} \left[x_i^2 - 10\cos(2\pi x_i) + 10\right]\right) + \sum_{i=1}^{n} u(x_i, 10, 100, 4)$ $u(x_i, a, k, m) = \begin{cases} k(-x_i - a)^m & \text{if } x_i < a \\ 0 & \text{if } -a \le x_i \le a \\ k(x_i - a)^m & \text{if } x_i > -a \end{cases}$	$[-50,\ 50]$	30	$[0, \ldots, 0]$	0

Table 2. Parameter settings for optimization algorithms.

Algorithm	Parameter	Value
GWO	Convergence factor	Decreases linearly from 2 to 0
BOA	Probability switch, sensory modality, power exponent	0.8, 0.01, 0.1
WOA	Convergence factor (a)	Decreases linearly from 2 to 0
MVO	Minimum and maximum likelihood of wormholes existing	0.1, 1.0
SSA	Exploration-Exploitation parameter	Decreases exponentially from 2 to 0
ALO	Parameter used in random walk of ants	2.0
SCA	Exploration-Exploitation parameter	Decreases exponentially from 2 to 0

Table 3. Statistical results for benchmark functions.

Function	Metrics	GWO	BOA	WOA	MVO	SSA	ALO	SCA	EO	LF-IEO
Sphere	Best	1.31×10^{-12}	1.87×10^{-9}	4.02×10^{-36}	1.34×10^{-2}	2.32×10^{-2}	6.71×10^{-2}	6.29×10^{-2}	5.35×10^{-18}	$\mathbf{0.00 \times 10^{0}}$
	Average	1.44×10^{-11}	4.10×10^{-9}	8.62×10^{-31}	2.13×10^{-2}	1.10×10^{-1}	2.19×10^{0}	1.95×10^{0}	1.88×10^{-16}	$\mathbf{0.00 \times 10^{0}}$
	Worst	3.84×10^{-11}	6.59×10^{-9}	8.74×10^{-30}	4.08×10^{-2}	3.29×10^{-1}	6.61×10^{0}	9.94×10^{0}	1.11×10^{-15}	$\mathbf{0.00 \times 10^{0}}$
	SD	1.82×10^{-11}	4.28×10^{-9}	2.31×10^{-30}	2.20×10^{-2}	1.28×10^{-1}	2.73×10^{0}	2.79×10^{0}	2.98×10^{-16}	$\mathbf{0.00 \times 10^{0}}$
	Rank	4	5	2	6	7	9	8	3	**1**
Schwefel	Best	6.75×10^{-3}	2.59×10^{-6}	1.36×10^{1}	3.07×10^{0}	1.08×10^{1}	1.38×10^{1}	1.70×10^{1}	6.40×10^{-5}	$\mathbf{0.00 \times 10^{0}}$
	Average	4.06×10^{-2}	4.25×10^{-6}	5.83×10^{1}	6.99×10^{0}	1.66×10^{1}	2.22×10^{1}	5.61×10^{1}	1.10×10^{-3}	$\mathbf{0.00 \times 10^{0}}$
	Worst	9.23×10^{-2}	5.22×10^{-6}	9.00×10^{1}	1.39×10^{1}	2.31×10^{1}	3.21×10^{1}	8.18×10^{1}	3.25×10^{-3}	$\mathbf{0.00 \times 10^{0}}$
	SD	4.66×10^{-2}	4.29×10^{-6}	6.30×10^{1}	7.42×10^{0}	1.68×10^{1}	2.25×10^{1}	5.73×10^{1}	1.46×10^{-3}	$\mathbf{0.00 \times 10^{0}}$
	Rank	4	2	9	5	6	7	8	3	**1**
Beale	Best	7.73×10^{-9}	5.12×10^{-5}	1.29×10^{-12}	1.20×10^{-7}	8.47×10^{-16}	1.37×10^{-15}	1.29×10^{-6}	$\mathbf{6.87 \times 10^{-30}}$	2.03×10^{-12}
	Average	5.08×10^{-2}	5.41×10^{-2}	5.08×10^{-2}	2.04×10^{-1}	7.62×10^{-2}	7.69×10^{-2}	8.67×10^{-4}	$\mathbf{1.57 \times 10^{-16}}$	2.12×10^{-9}
	Worst	7.63×10^{-1}	2.57×10^{-1}	7.63×10^{-1}	7.63×10^{-1}	7.63×10^{-1}	7.83×10^{-1}	3.05×10^{-3}	$\mathbf{4.43 \times 10^{-15}}$	2.49×10^{-8}
	SD	1.96×10^{-1}	8.77×10^{-2}	1.96×10^{-1}	3.94×10^{-1}	2.42×10^{-1}	2.43×10^{-1}	1.09×10^{-3}	$\mathbf{8.10 \times 10^{-16}}$	5.39×10^{-9}
	Rank	5	6	4	9	7	8	3	**1**	2
Ackley	Best	6.48×10^{-6}	2.58×10^{-6}	3.55×10^{-15}	2.10×10^{0}	3.21×10^{0}	1.14×10^{1}	2.35×10^{0}	4.89×10^{-9}	$\mathbf{0.00 \times 10^{0}}$
	Average	1.76×10^{-5}	4.33×10^{-6}	3.02×10^{-14}	2.86×10^{0}	4.90×10^{0}	1.39×10^{1}	6.06×10^{0}	4.56×10^{-8}	$\mathbf{0.00 \times 10^{0}}$
	Worst	4.93×10^{-5}	6.11×10^{-6}	1.21×10^{-13}	4.35×10^{0}	9.06×10^{0}	1.58×10^{1}	1.09×10^{1}	1.73×10^{-7}	$\mathbf{0.00 \times 10^{0}}$
	SD	1.99×10^{-5}	4.39×10^{-6}	4.06×10^{-14}	2.92×10^{0}	5.10×10^{0}	1.41×10^{1}	6.43×10^{0}	5.96×10^{-8}	$\mathbf{0.00 \times 10^{0}}$
	Rank	5	4	2	6	7	9	8	3	**1**
Rastrigin	Best	4.32×10^{0}	3.68×10^{-9}	0.00×10^{0}	8.72×10^{1}	3.00×10^{1}	6.12×10^{1}	1.56×10^{1}	1.71×10^{-13}	$\mathbf{0.00 \times 10^{0}}$
	Average	1.65×10^{1}	4.07×10^{1}	2.27×10^{-14}	1.41×10^{2}	5.85×10^{1}	9.04×10^{1}	9.88×10^{1}	6.65×10^{-2}	$\mathbf{0.00 \times 10^{0}}$
	Worst	4.60×10^{1}	2.20×10^{2}	2.84×10^{-13}	2.10×10^{2}	9.00×10^{1}	1.39×10^{2}	2.18×10^{2}	9.99×10^{-1}	$\mathbf{0.00 \times 10^{0}}$
	SD	1.86×10^{1}	9.10×10^{1}	6.88×10^{-14}	1.45×10^{2}	6.09×10^{1}	9.28×10^{1}	1.12×10^{2}	2.58×10^{-1}	$\mathbf{0.00 \times 10^{0}}$
	Rank	4	5	2	9	6	7	8	3	**1**
Griewank	Best	1.81×10^{-9}	2.58×10^{-9}	0.00×10^{0}	1.04×10^{0}	1.09×10^{0}	1.41×10^{0}	1.22×10^{0}	7.33×10^{-15}	$\mathbf{0.00 \times 10^{0}}$
	Average	6.44×10^{-3}	8.07×10^{-9}	4.14×10^{-2}	1.08×10^{0}	1.59×10^{0}	9.42×10^{0}	6.98×10^{0}	1.97×10^{-3}	$\mathbf{0.00 \times 10^{0}}$
	Worst	3.71×10^{-2}	1.46×10^{-8}	7.21×10^{-1}	1.12×10^{0}	4.22×10^{0}	2.62×10^{1}	2.70×10^{1}	5.93×10^{-2}	$\mathbf{0.00 \times 10^{0}}$
	SD	1.28×10^{-2}	8.57×10^{-9}	1.62×10^{-1}	1.07×10^{0}	1.74×10^{0}	1.21×10^{1}	9.17×10^{0}	1.08×10^{-2}	$\mathbf{0.00 \times 10^{0}}$
	Rank	4	2	5	6	7	9	8	3	**1**

Table 3. *Cont.*

Function	Metrics	GWO	BOA	WOA	MVO	SSA	ALO	SCA	EO	LF-IEO
Shekel	Best	$\mathbf{2.59 \times 10^{-3}}$	5.60×10^{0}	7.92×10^{-3}	4.71×10^{-5}	-1.59×10^{-4}	-1.59×10^{-4}	4.06×10^{0}	-1.59×10^{-4}	-1.57×10^{-4}
	Average	$\mathbf{4.42 \times 10^{-1}}$	6.67×10^{0}	3.67×10^{0}	1.45×10^{0}	2.52×10^{0}	4.89×10^{0}	7.05×10^{0}	1.88×10^{0}	6.47×10^{-1}
	Worst	$\mathbf{6.47 \times 10^{0}}$	8.11×10^{0}	8.68×10^{0}	7.75×10^{0}	8.04×10^{0}	8.68×10^{0}	9.98×10^{0}	7.93×10^{0}	6.47×10^{0}
	SD	$\mathbf{1.67 \times 10^{0}}$	6.70×10^{0}	4.83×10^{0}	3.04×10^{0}	4.18×10^{0}	5.91×10^{0}	7.18×10^{0}	3.46×10^{0}	2.04×10^{0}
	Rank	**1**	8	6	3	5	7	9	4	2
Penalized	Best	2.91×10^{0}	0.00×10^{0}	0.00×10^{0}	1.76×10^{2}	3.19×10^{2}	7.50×10^{2}	5.20×10^{2}	1.94×10^{-12}	$\mathbf{0.00 \times 10^{0}}$
	Average	2.12×10^{1}	1.28×10^{-10}	1.66×10^{-15}	2.69×10^{2}	7.26×10^{2}	1.53×10^{3}	6.74×10^{6}	6.60×10^{-1}	$\mathbf{0.00 \times 10^{0}}$
	Worst	3.94×10^{1}	8.94×10^{-10}	2.84×10^{-14}	4.19×10^{2}	1.94×10^{3}	4.42×10^{3}	4.17×10^{7}	4.60×10^{0}	$\mathbf{0.00 \times 10^{0}}$
	SD	2.28×10^{1}	2.55×10^{-10}	5.37×10^{-15}	2.74×10^{2}	8.09×10^{2}	1.68×10^{3}	1.32×10^{7}	1.41×10^{0}	$\mathbf{0.00 \times 10^{0}}$
	Rank	5	3	2	6	7	8	9	4	**1**
Overall Ranking		3	4	3	5	6	8	7	2	**1**

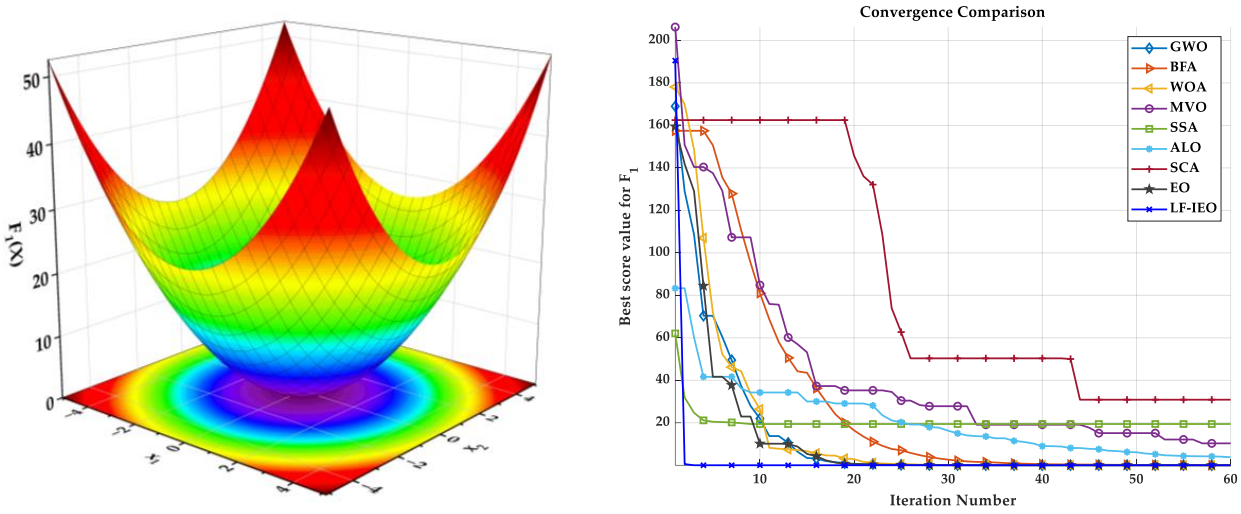

(**a**) (**b**)

Figure 3. (**a**) Graphical representation of F_1; (**b**) Comparison of convergence curve for F_1.

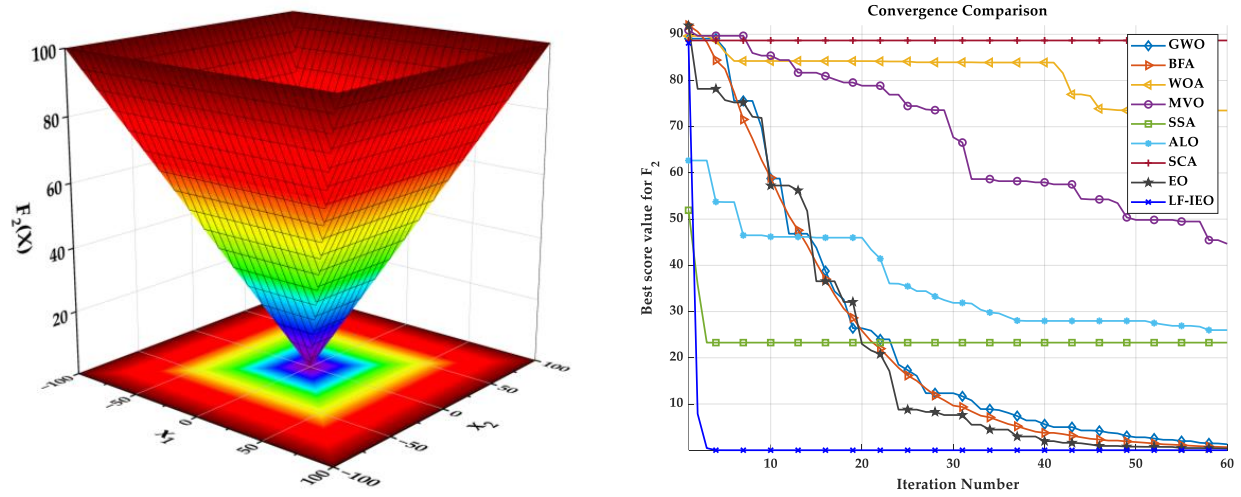

(**a**) (**b**)

Figure 4. (**a**) Graphical representation of F_2; (**b**) Comparison of convergence curve for F_2.

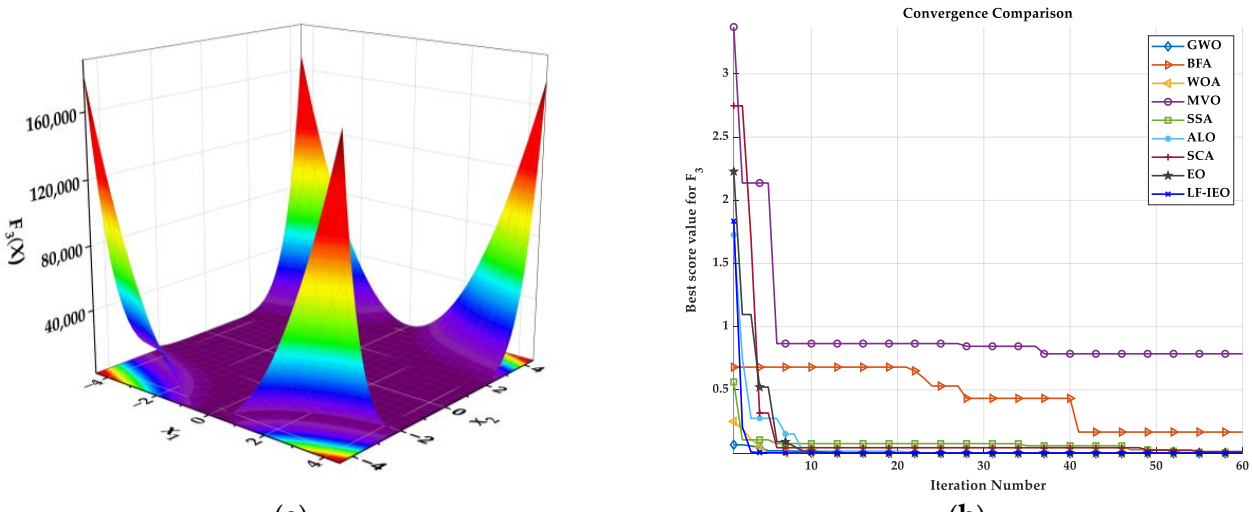

(**a**) (**b**)

Figure 5. (**a**) Graphical representation of F_3; (**b**) Comparison of convergence curve for F_3.

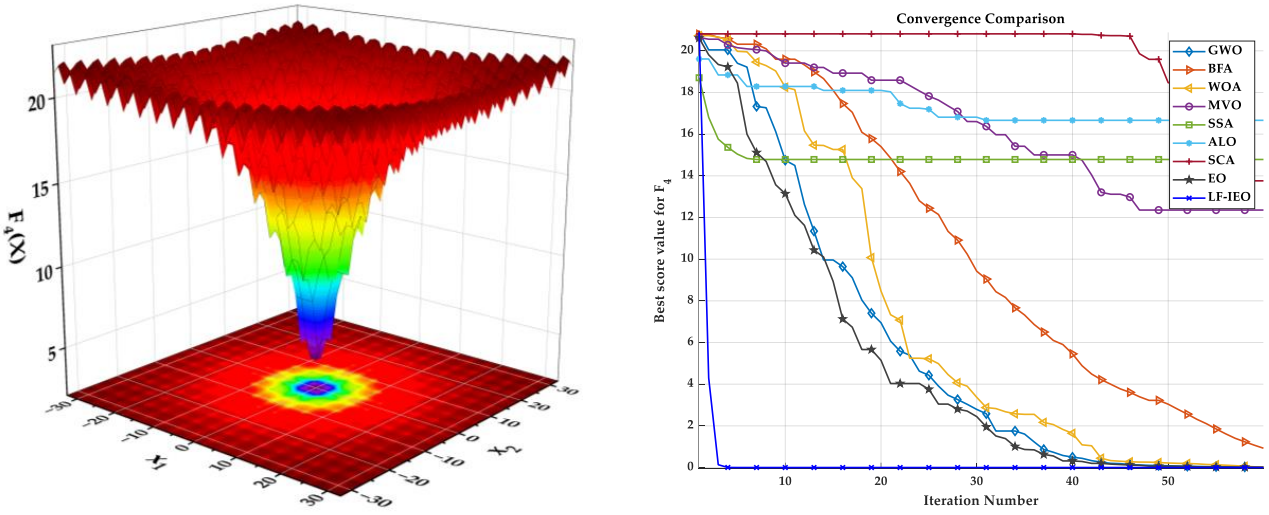

(**a**) (**b**)

Figure 6. (**a**) Graphical representation of F_4; (**b**) Comparison of convergence curve for F_4.

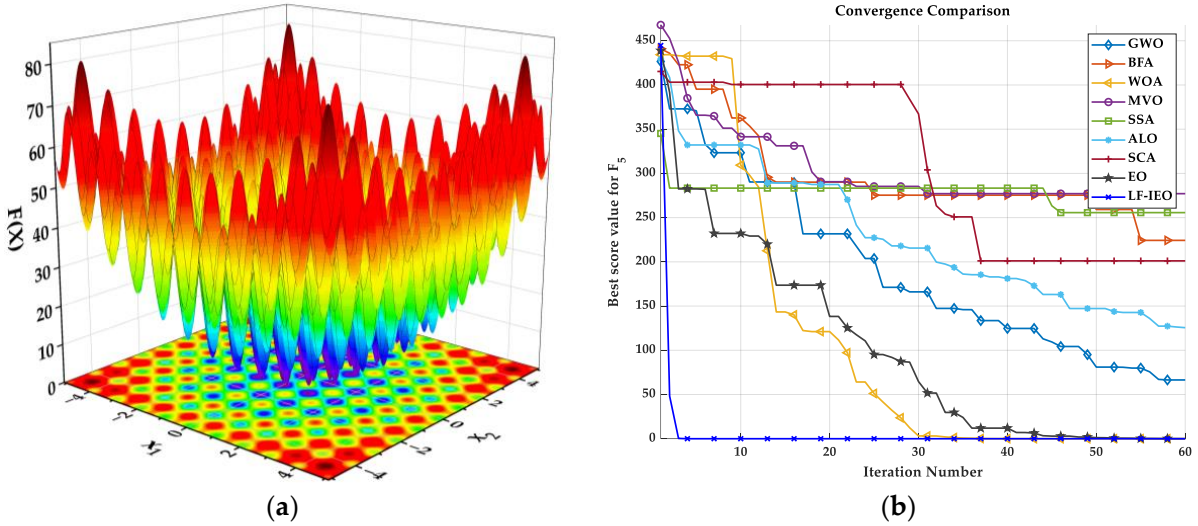

(**a**) (**b**)

Figure 7. (**a**) Graphical representation of F_5; (**b**) Comparison of convergence curve for F_5.

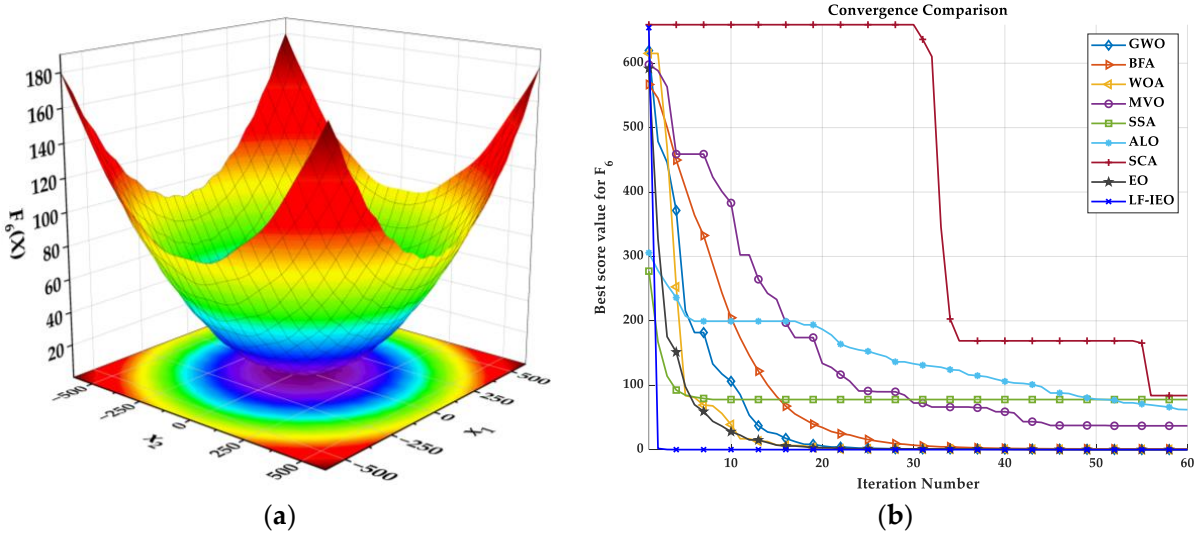

(**a**) (**b**)

Figure 8. (**a**) Graphical representation of F_6; (**b**) Comparison of convergence curve for F_6.

Integrating the GPS initialization, Lévy Flight strategy, FROBL, and the introduction of an oscillating Generation Probability in the position update equation have significantly enhanced LF-IEO's ability to balance exploration and exploitation. This synergistic combination allows LF-IEO to navigate the solution space efficiently, avoiding premature convergence and consistently finding high-quality solutions. The improved performance is particularly evident in functions with numerous local optima, demonstrating LF-IEO's enhanced capacity to escape local minima and continue exploring the search space effectively. These results underscore LF-IEO's competence in providing superior optimization outcomes across a diverse range of problem landscapes, establishing it as a powerful and versatile algorithm for complex optimization tasks.

3. Problem Formulation

3.1. SOPs Modeling

Distribution systems consist of two types of branches: sectionalizing switches (normally closed condition, NCC) and tie switches (normally open point, NOP). Optimal network reconfiguration in these systems traditionally involves changing the open/closed status of these switches to achieve objectives such as loss reduction and voltage profile improvement while maintaining radial topology. However, an emerging alternative to opening tie switches is the use of SOPs. First proposed in 2011 [38], SOPs are power electronic devices that provide flexible power flow control between feeders. Unlike mechanical switches, SOPs allow continuous and independent control of active and reactive power flows, enhancing operational flexibility. Various SOP topologies exist, such as Back-to-Back Voltage Source Converters (VSCs), a Static Series Synchronous Compensator (SSSC), and a Unified Power Flow Controller (UPFC) [18]. The Back-to-Back VSC configuration is considered in this work due to its widespread application and operational advantages. The back-to-back VSC topology, shown in Figure 1, consists of two VSCs connected via a DC link. This arrangement enables four-quadrant power flow control between the connected AC feeders, fault isolation, and voltage support.

The total active power output from the SOPs converters, along with their internal power losses, must collectively sum to zero, as represented by [39,40]:

$$P_{SOP}^{inj,I} + P_{SOP}^{inj,II} + P_{SOP}^{Loss,I} + P_{SOP}^{Loss,II} = 0 \tag{10}$$

where $P_{SOP}^{inj,I}$ and $P_{SOP}^{inj,II}$ represent the injected active power at terminals *I* and *II*, respectively. The power losses at terminals *I* and *II* of the SOP are defined by:

$$\begin{cases} P_{SOP}^{Loss,I} = A_{SOP}\sqrt{P_{SOP}^{inj,I} + Q_{SOP}^{inj,I}} \\ P_{SOP}^{Loss,II} = A_{SOP}\sqrt{P_{SOP}^{inj,II} + Q_{SOP}^{inj,II}} \end{cases} \tag{11}$$

where $Q_{SOP}^{inj,I}$ and $Q_{SOP}^{inj,II}$ represent the injected reactive power at terminals *I* and *II* of the SOP, respectively, and A_{SOP} denotes the loss coefficient of the two converters of the SOP at nodes terminals *I* and *II* [41]. A_{SOP} is taken in this paper as 0.01.

3.2. Objective Function

The economic objective of the simultaneous placement of SOPs and network reconfiguration in radial distribution systems is to maximize the Total Net Revenue (*TNR*) while satisfying equality and inequality constraints. To achieve this using minimization-based optimization algorithms, the objective function is formulated as follows:

$$min \;\; F_{obj} = 1/TNR \tag{12}$$

where TNR is defined as:

$$TNR = K_P\left(T \times P_{TLoss}^{Before}\right) - \left\{K_P\left(T \times P_{TLoss}^{After}\right) + \left(Cost_{SOP}^{INV}\right) + \left(Cost_{SOP}^{MNT}\right)\right\} (\$/\text{year}) \quad (13)$$

Here, K_P is the cost of power losses taken in this paper as 0.114 \$/kWh [42], T is the time period (equivalent to 8760 h annually), P_{TLoss}^{Before} and P_{TLoss}^{After} are power losses before and after optimization, respectively, $Cost_{SOP}^{INV}$ is the annual investment cost of SOPs, and $Cost_{SOP}^{MNT}$ is the annual maintenance cost of SOPs. Note that the power losses are calculated based on the maximum load scenario.

Total power losses P_{TLoss} within a distribution system may be calculated through the following equation:

$$P_{TLoss} = \sum_{i=1}^{N_{bus}} \sum_{j=1}^{N_{bus}} G_{ij}[V_i^2 + V_j^2 - 2V_iV_j\cos\theta_{ij}] \quad (14)$$

where G_{ij} is the real part of the admittance matrix, V_i and V_j are the voltage magnitudes at buses i and j, θ_{ij} is the voltage angle difference between buses i and j, and N_{bus} is the total number of buses in the network.

The investment cost of SOPs per year is computed below [8,12]:

$$Cost_{SOP}^{INV} = \left(\frac{(1+B)^n \times B}{(1+B)^n - 1}\right) \times \sum_{i=1}^{N_{SOP}} c_{SOP} \times S_{SOP_i} \quad (15)$$

where c_{SOP} is the cost per unit capacity of SOPs, S_{SOP_i} is the capacity of the ith SOP, N_{SOP} is the number of installed SOPs, n is the lifetime of the SOPs in years, and B is the rate of return. In this paper: $c_{SOP} = 200$ \$/kVA, $n = 30$, and $B = 0.05$ [10].

The maintenance cost of SOPs per year:

$$Cost_{SOP}^{MNT} = \eta \times \sum_{i=1}^{N_{SOP}} c_{SOP} \times S_{SOP_i} \quad (16)$$

where η is the coefficient of the annual maintenance cost of SOPs taken in this paper as 0.02 [10].

3.3. System Constraints

The proposed optimization problem is subject to several critical constraints. These constraints ensure the feasibility and reliability of the proposed solutions while adhering to the physical limitations of the power system. The key constraints can be categorized into three main groups: power flow equations, voltage profile constraints, and branch flow limits.

A. Power Flow Equations

The power flow equations represent the fundamental physical laws governing the operation of electrical power systems. These equations ensure that the power injected into each bus equals the power flowing out, accounting for losses and demand. For each bus in the system, the following conditions must be satisfied:

(a) Net Active Power Balance:

$$P_{Li} + V_i\sum_{j=1}^{N_{bus}} V_j\left(G_{ij}\cos\theta_{ij} + B_{ij}\sin\theta_{ij}\right) = 0 \quad (17)$$

(b) Net Reactive Power Balance:

$$Q_{Li} + V_i\sum_{j=1}^{N_{bus}} V_j\left(G_{ij}\sin\theta_{ij} - B_{ij}\cos\theta_{ij}\right) = 0 \quad (18)$$

where P_{Li} and Q_{Li} are the active and reactive power load at bus i.

B. Voltage Profile Constraints

Maintaining the proper voltage level is crucial for the operation of electrical equipment connected to the distribution system. The voltage at each bus must remain within an acceptable range, typically ±5% of the nominal voltage [1]:

$$V^{\min} \leq V_i \leq V^{\max} \tag{19}$$

where $V^{\min}$ is the lower voltage limit (0.95 per unit), and $V^{\max}$ is the upper voltage limit (1.05 per unit).

C. Branch Flow Limits:

To maintain the safety of the branches in a distribution system and prevent overloading, which could lead to overheating, the current flowing through each branch must not exceed its maximum permissible limit. This constraint is expressed as:

$$I_{i,j} = \sqrt{\left(G_{ij}^2 + B_{ij}^2\right)\left(V_i^2 + V_j^2 - 2V_iV_j\cos\theta_{ij}\right)} \leq I_{i,j}^{\max} \tag{20}$$

where $I_{i,j}$ is the magnitude of the current flowing from bus i to bus j.

D. Operating constraints of SOPs

The apparent power flowing through the SOP must not exceed the SOP's rated capacity to prevent overloading and ensure safe operation [9,40,43]. The constraint is expressed as:

$$\begin{cases} \sqrt{P_{SOP}^{inj,I} + Q_{SOP}^{inj,I}} \leq S_{SOP} \\ \sqrt{P_{SOP}^{inj,II} + Q_{SOP}^{inj,II}} \leq S_{SOP} \end{cases} \tag{21}$$

where S_{SOP} denotes the rated apparent power capacity of the SOP.

3.4. Constraints Handling Techniques

Effectively managing these constraints is crucial for finding optimal solutions. In this study, we employ a combination of methods to handle different types of constraints:

A. Equality Constraints

The power flow equations, which are equality constraints, are inherently satisfied through the Backward-Forward Load Flow (BFLF) convergence [44]. This method offers benefits such as implementation simplicity, high computational performance, stable convergence, and minimal memory use. Most importantly, it efficiently handles networks with high R/X ratios (resistance to reactance ratios). It iteratively solves the power flow equations until a satisfactory level of convergence is achieved, ensuring power balance throughout the network. Algorithm 4 presents a BFLF method that incorporates SOPs. This algorithm employs the Branch Current to Bus Voltage (BCBV) and the Bus Injection to Branch Current (BIBC) matrices, whose formulation and calculation are detailed in [45].

Algorithm 4: Backward-Forward Load Flow Method with SOPs

Input: *BIBC* matrix, *BCBV* matrix, bus data, branch data, tolerance ε, itr_{max} (Iteration limit)

Output: V (Bus voltages), I_{br} (Branch currents), P_{TLoss} (Total power losses)

Initialize bus voltages V to 1.0 p.u.
itr = 1, converged = false,
for *each branch (i,j) containing a SOP* **do**
    Update active power injections at buses *i* and *j* due to SOP power transfer:
    $P_{Li} = P_{Li} - P_{SOP}^{inj,I}$, $P_{Lj} = P_{Lj} - P_{SOP}^{inj,II}$
    Update reactive power injections at buses *i* and *j* due to SOP power transfer:
    $Q_{Li} = Q_{Li} - Q_{SOP}^{inj,I}$, $Q_{Lj} = Q_{Lj} - Q_{SOP}^{inj,II}$
end
while (not converged) **and** ($itr < itr_{max}$) **do**
    for $i = 1$ *to* N_{bus} **do**
        Calculate the nodal current injection:
        $I_{inj}^{iter}(i) = conj\left(\left(P_{Li} + jQ_{Li}\right)/V_i^{(k-1)}\right) + \left(jB_i V_i^{(k-1)}/2\right)$
    end
    // Backward sweep using *BIBC* matrix
    $I_{br}^{iter} = \left[BIBC\right] \times \left[I_{inj}^{iter}\right]$
    // Forward sweep using *BCBV* matrix
    $V^{iter} = \left[BCBV\right] \times I_{br}^{iter}$
    if $max\left(\left|V^{iter} - V^{iter-1}\right|\right) < \varepsilon$ then
        converged = true
    end
    $itr = itr + 1$
end
Calculate the total power losses using Equation (14)
Return V, I_{br}, P_{TLoss}

B. Inequality Constraints

In this paper, for handling inequality constraints, such as voltage profile constraints, branch flow limits, and the operating limits of SOPs, the penalty function method is adopted [46]. This approach incorporates the constraints into the objective function by adding penalty terms for any violations. The modified objective function takes the following form:

$$F_{obj}^{P} = F_{obj} + \zeta \times (h_V + h_I + h_{SOP}) \quad (22)$$

where F_{obj}^{P} is the penalized objective function, F_{obj} is the original objective function defined in Equation (12), ζ is a large penalty factor (set to 10,000 in this study), h_I, h_V, h_{SOP} and are penalty terms for constraint violations. The penalty terms are defined as follows:

$$h_V = \sum_{i=1}^{N_{bus}} \left\{ max(0,\ V_i - V^{\max})^2 + max\left(0,\ V^{\min} - V_i\right)^2 \right\} \tag{23}$$

$$h_I = \sum_{i,j} max\left(0,\ I_{i,j}^{\max} - I_{i,j}\right)^2 \tag{24}$$

$$h_{SOP} = \sum_{i=1}^{N_{SOP}} \left\{ \begin{array}{l} max\left(0,\ \sqrt{P_{SOP,i}^{inj,I} + Q_{SOP,i}^{inj,I}} - S_{SOP,i}\right)^2 + \\ max\left(0,\ \sqrt{P_{SOP,i}^{inj,II} + Q_{SOP,i}^{inj,II}} - S_{SOP,i}\right)^2 \end{array} \right\} \tag{25}$$

This formulation ensures that any violation of branch flow limits, voltage constraints, or SOPs operating limits results in a significant increase in the objective function value, steering the optimization algorithm away from infeasible solutions.

4. Application of LF-IEO in the Proposed Problem

4.1. Encoding/Decoding Solutions

A. Encoding process

The encoding process of solutions is a crucial component in solving optimization problems. Many previous studies focusing on metaheuristic approaches for reconfiguration in distribution networks have typically employed two main encoding strategies for candidate solutions: (a) a binary vector representing the status (open/closed) of each branch or (b) an integer vector identifying the indices of open branches. While these methods have been widely used, they often result in a significant number of infeasible solutions that violate the fundamental radial structure requirement of distribution networks, known in graph theory as a spanning tree. Such violations can manifest as loops or isolated buses. Consequently, these encoding approaches may lead to slower convergence or even non-optimal solutions due to the time spent evaluating and discarding infeasible configurations [47].

In contrast, this paper proposes an approach utilizing a continuous encoding scheme with real numbers. This method represents potential solutions as a vector X, which contains real numbers between 0 and 1 corresponding to the weights of all branches in the system, as well as the SOPs parameters. Figure 9 illustrates an example of a randomly generated solution for an 11-bus/13-branch network with one SOP, demonstrating the structure and composition of this encoding scheme. In this method, both the branch weights and SOP sizes are normalized within the 0 to 1 range.

Figure 9. Structure of the encoded solution X vector.

B. Decoding process

The decoding process, as detailed in Algorithm 5, is grounded in graph theory and employs Kruskal's method [48] for finding a minimum spanning tree. In graph theory, a spanning tree refers to a subset of edges (branches in this context) that connects all vertices (buses) without forming any loops. This concept is crucial for maintaining the radial structure essential to distribution networks and the optimization process.

The algorithm begins by constructing the spanning tree based on the weights encoded in the solution vector X. Once this radial configuration is established, the remaining branches are identified as "*DeactiveBranches*", representing potential positions for SOPs placement. SOP positions are then selected from among these "*DeactiveBranches*" based on the lowest weights, optimizing their placement within the network. Finally, the SOP sizes are extracted from the corresponding elements in the original solution vector X. This step completes the decoding process, resulting in a fully specified radial configuration with the corresponding SOP positions and sizes. Figure 10 illustrates the decoding process, showing how the algorithm constructs the radial configuration and places SOPs for the example presented in Figure 9. The solid lines depict the active branches forming the radial configuration, while the dotted lines depict the deactivated branches.

Algorithm 5: Decoding Solutions

Input: X (X is a possible solution containing weights corresponding to all branches and SOPs parameters)

Output: The radial configuration with SOPs positions and sizes.

```
Create an empty list called "ActiveBranches" to store the final configuration
Sort all branches in ascending order of their weights
Create a separate group for each bus in the system
for each branch in the sorted branch list do
    Identify the two buses connected by this branch
    if these buses belong to different groups do
        Add this branch to "ActiveBranches"
        Merge the groups of these two buses
    end
    if Number of branches in "ActiveBranches" = (total number of buses - 1) then
        Break the for loop
    end
end
Identify remaining branches as "DeactiveBranches" as potential SOPs positions.
Select SOPs positions among "DeactiveBranches" based on the lowest weights
Extract SOPs sizes from the corresponding elements in X
Return the radial configuration with SOPs positions and sizes
```

It is worth mentioning that during the decoding process, each SOP sizing parameter ($P_{SOP}^{inj,I}$, $Q_{SOP}^{inj,I}$, and $Q_{SOP}^{inj,II}$) is obtained directly from the solution vector. However, $P_{SOP}^{inj,II}$ is calculated using a non-linear numerical method such as Newton-Raphson [49], from Equations (10) and (11).

The advantages of this encoding/decoding technique are threefold: (a) the encoded solutions are represented as vectors of real numbers between 0 and 1, which simplifies the optimization process; (b) it ensures a unique configuration for each distinct potential solution; and (c) it avoids invisible solutions by constructing the solution from a minimum spanning tree, thus guaranteeing a radial network structure (no loops or isolated buses).

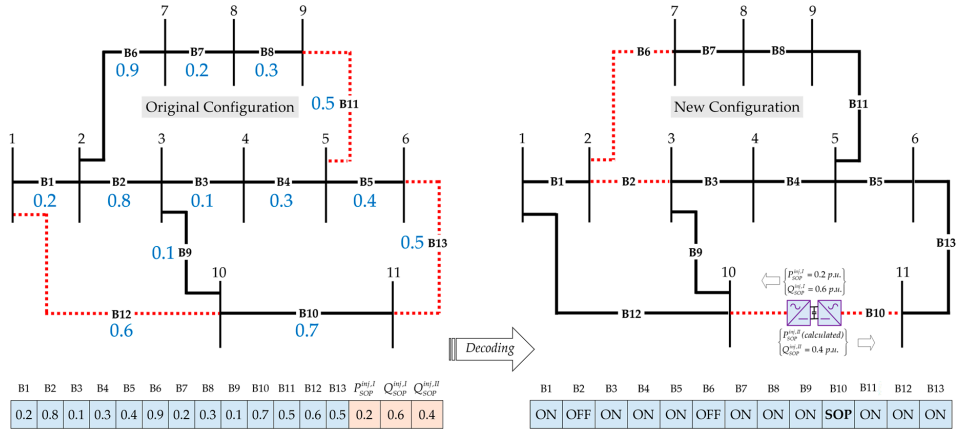

Figure 10. Illustration of the decoding process for radial configuration and SOPs placement.

4.2. Flowchart Description of the LF-IEO Algorithm Process

Figure 11 presents a comprehensive flowchart of the LF-IEO algorithm, illustrating the step-by-step process designed for optimizing the simultaneous placement of SOPs and network reconfiguration in radial distribution systems.

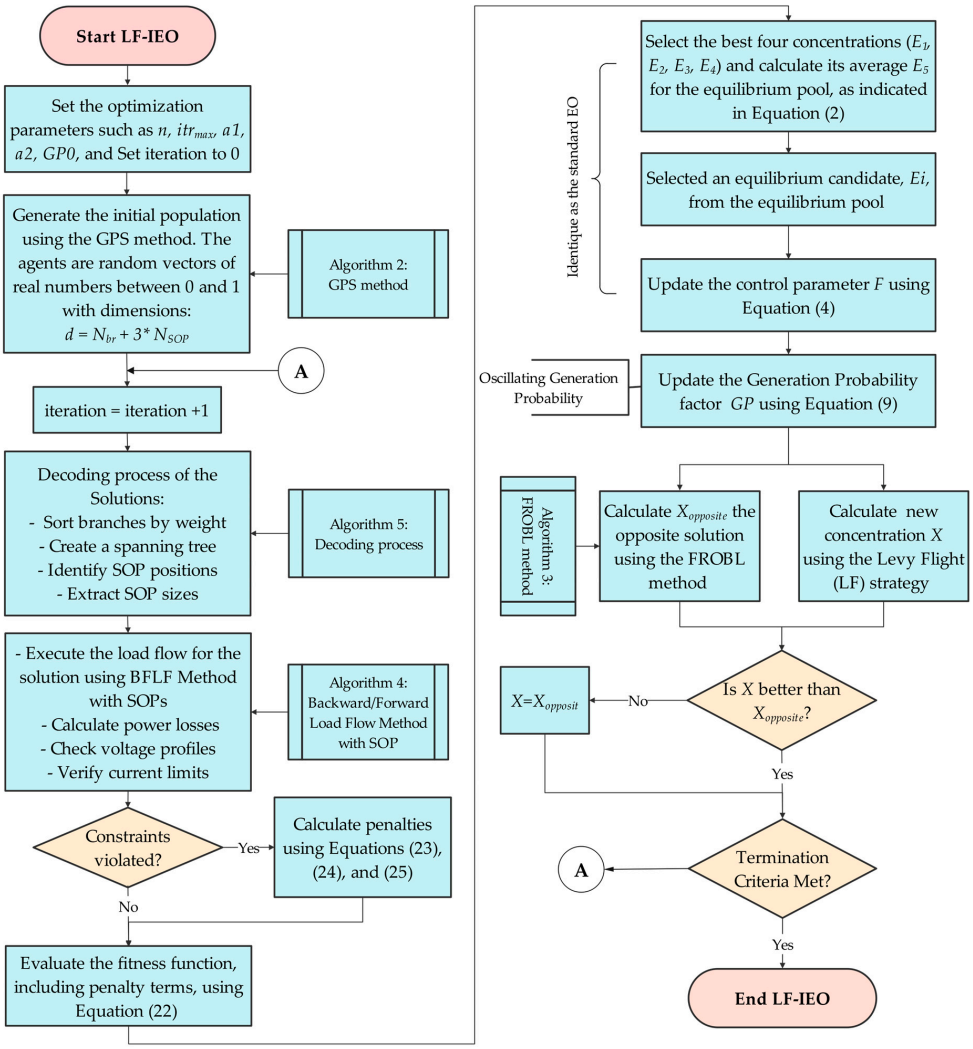

Figure 11. Flowchart of the LF-IEO algorithm for simultaneous SOPs Placement and Network Reconfiguration.

The algorithm begins with the initialization of optimization parameters and the generation of an initial population using the GPS method. The main iterative process includes key steps such as decoding solutions, executing load flow analysis, and evaluating the fitness function with penalty terms for constraint violations. The flowchart highlights the unique features of LF-IEO, including equilibrium pool selection, the calculation of GP using an oscillating function, and the incorporation of the LF strategy for enhanced exploration. Additionally, the FROBL method is applied to generate opposite solutions, potentially improving the algorithm's convergence. This iterative process continues until termination criteria are met, ensuring an optimal or near-optimal solution for SOP placement and network reconfiguration. Overall, the flowchart effectively captures the algorithm's structure, showcasing its capacity to balance exploration and exploitation in complex optimization scenarios.

5. Simulation Results and Discussion

The efficacy of the LF-IEO algorithm was initially verified on various benchmark functions, as detailed in a previous section. These benchmark tests demonstrated the algorithm's robustness and effectiveness across a range of optimization problems, establishing a solid foundation for its application to more complex, real-world scenarios. Building on these promising results, the LF-IEO algorithm was subsequently applied to the proposed problem of simultaneous SOP placement and reconfiguration in radial distribution networks. The algorithm's performance was rigorously evaluated on three distinct distribution networks: the IEEE 33-bus, 69-bus, and 118-bus standard systems, along with an Algerian 116-bus system. In each case, a specific number of SOPs were considered: two for the 33-bus system, two for the 69-bus system, four for the 118-bus system, and three for the Algerian 116-bus system. The simulations were conducted using MATLAB 2024a software (24.1.0)on a PC equipped with an Intel Core i9-14700K processor (5.60 GHz clock frequency) and 64 GB of memory, running on the Windows 11 operating system. Table 4 outlines the key parameters employed in the LF-IEO algorithm for each test system. These parameters were carefully tuned to balance computational efficiency with solution quality across the different network sizes.

Table 4. Parameters of LF-IEO method.

Parameter	33-Bus	69-Bus	118-Bus	Algerian 116-Bus
Population Size	200	500	1000	1000
Max Iterations of LF-IEO	500	1000	2000	2000
a1, a2, GP0	2.0, 1.0, 0.5	2.0, 1.0, 0.5	2.0, 1.0, 0.5	2.0, 1.0, 0.5
Maximum Load Flow Iterations	50	50	50	50
Load Flow Convergence Tolerance	1×10^{-5}	1×10^{-5}	1×10^{-5}	1×10^{-5}
Number of SOPs	2	2	4	3
Minimum and Maximum SOP sizes	0.1, 1.0 MVAr	0.1, 1.0 MVAr	0.1, 1.0 MVAr	0.1, 1.0 MVAr

5.1. IEEE 33-Bus Test System

The initial tested network is a 33-bus radial distribution system composed of 37 branches, 32 switches in the closed position, and 5 switches in the open position corresponding to branches {33, 34, 35, 36, 37}. This network operates at a base voltage of 12.66 kV and an apparent power of 10 MVA. In the base case, without any reconfiguration or SOPs installation, the system experiences an active power loss of 202.68 kW, resulting in an annual cost of 202,401.48 $/year. The minimum voltage observed at bus 18 is 0.91309 p.u., which is substantially below the lower acceptable limit of 0.95 p.u. Detailed system information can be found in [50]. It is assumed that the maximum permissible current of all branches is 255 A [51].

Table 5 illustrates the results of applying the proposed LF-IEO algorithm to the IEEE 33-Bus System. The table compares three scenarios: the base case, optimal reconfiguration without SOPs, and simultaneous optimal reconfiguration with SOPs placement. The most

significant improvements are achieved when combining optimal reconfiguration with strategic SOP deployment. This approach reduces power losses by 45.47% compared to the base case, resulting in a total power loss of 110.52 kW, including SOP losses. Importantly, the minimum voltage is raised to 0.95588 p.u., effectively addressing the low voltage condition observed in the base case (below 0.95 p.u.).

Table 5. IEEE 33-Bus Network Results.

Outputs	Base Case	Optimal Reconfiguration	Optimal Reconfiguration with SOPs Placement
Open switches	33, 34, 35, 36, 37	7, 9, 14, 32, 37	7, 9, 14
Optimal SOP locations (branches)	-	-	32, 37
Optimal SOP sizes: $\{P_{SOP}^{inj,I}(kW), Q_{SOP}^{inj,I}(kVAr), P_{SOP}^{inj,II}(kW), Q_{SOP}^{inj,II}(kVAr)\}$	-	-	SOP_1 {−148.70, 270.27, 142.09, 322.23} SOP_2 {−16.09, 214.90, 12.20, 172.98}
Total power loss (kW)	202.68	139.55	110.52
Minimum Voltage (p.u.)	0.91309 (Below limit)	0.93782 (Below limit)	0.95588 (Within limit)
Maximum Voltage (p.u.)	1.00000	1.00000	1.00000
Cost of total loss ($/year)	202,401.48	139,360.43	110,367.10
SOPs investment and maintenance cost ($/year)	-	-	12,699.00
Net Saving ($/year)	-	63,041.05	79,335.38

Furthermore, this optimal configuration yields substantial economic benefits. Even after accounting for the annual SOPs investment and maintenance costs of 12,699.00 $/year, a net annual saving of $79,335.38 is realized. The simultaneous optimization of SOPs placement and open switch selection via the LF-IEO method not only minimizes power losses but also significantly enhances voltage quality and the overall capacity of the distribution network. This net saving reflects the favorable balance between reduced total loss costs and the expenditures associated with SOPs integration, thereby underscoring the economic viability and effectiveness of the LF-IEO method in optimizing distribution network performance.

The benefits of the LF-IEO method are further illustrated in Figure 12. This graph shows the voltage profiles across different bus numbers for the three scenarios. It clearly demonstrates that in the base case (blue line), several buses experience voltages below the acceptable minimum limit of 0.95 p.u., indicating significant voltage regulation issues. This problem is particularly severe in buses 6–18 and 26–33, where voltages drop well below the limit. In contrast, the reconfiguration with SOPs placement (green line) maintains voltages consistently above the 0.95 p.u. threshold across all buses, effectively addressing this voltage drop issue. The reconfiguration without SOPs (orange line) shows improvement over the base case but still struggles to maintain voltages above the limit for all buses.

Figure 13 illustrates the topology of the IEEE 33-bus distribution system, showing the bus connections and the locations of the switches and SOPs in the optimal configuration. The results provide clear evidence of the proposed LF-IEO algorithm's ability to optimize the overall system performance, both technically and economically. This is achieved by reducing power losses, balancing loads more effectively, mitigating potential stress points in the distribution network, and maximizing the net saving.

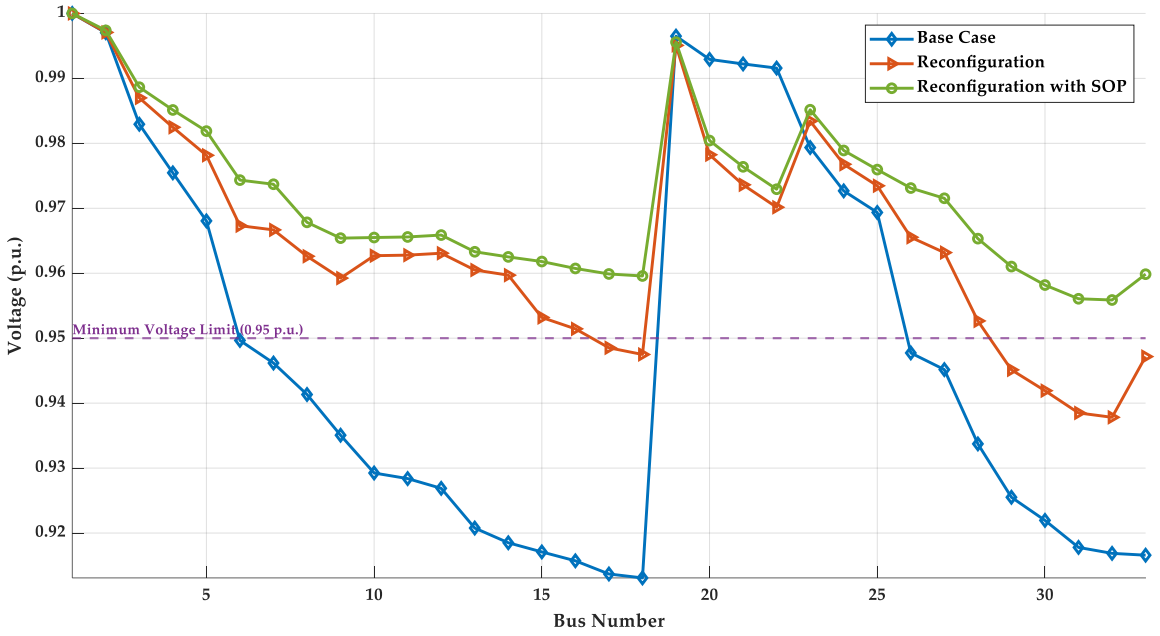

Figure 12. Voltage Profile Comparison for IEEE 33-Bus System.

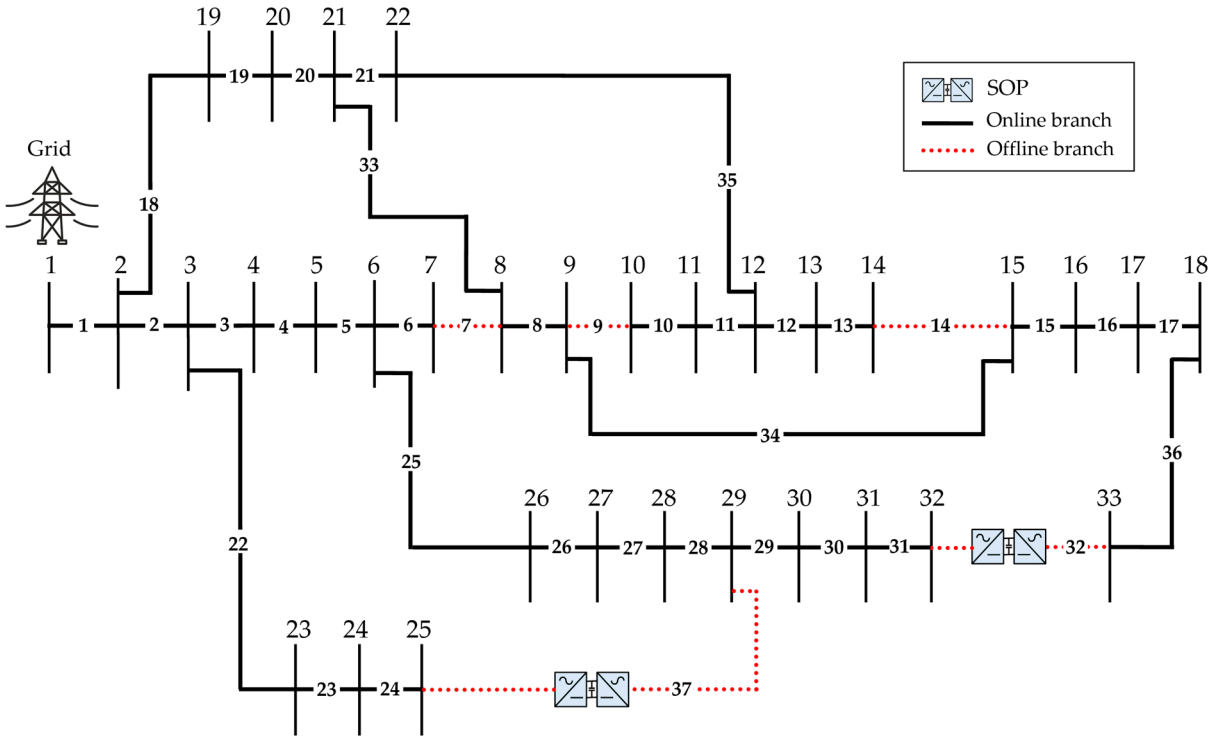

Figure 13. Optimal configuration of the IEEE 33-bus distribution system with SOPs placements.

5.2. IEEE 69-Bus Test System

The IEEE 69-bus system [52] was further used as a medium-scale radial distribution system to test the proposed LF-IEO algorithm. This test system includes 69 buses, 73 branches, and 68 sectionalizing switches, along with 5 tie switches. The initial configuration has open switch positions at branches {69, 70, 71, 72, 73}. System parameters include a capacity base of 1 MVA and a voltage base of 12.66 kV. The network carries a total load demand of 3.80 MW and 2.69 MVAR, with initial total losses of 224.76 kW, equating to an annual cost of 224,451.37 $/year. The voltage profile ranges from a minimum of 0.90919 p.u. at bus 65 to a high of 1.0 p.u. at the source bus.

Table 6 presents a comparison between the base case and optimized configuration of the IEEE 69-bus system, revealing significant improvements across various metrics. The simultaneous optimal network reconfiguration with SOPs location has changed open switches from {69, 70, 71, 72, 73} to {14, 69, 70}, with optimal SOPs locations identified at buses 56 and 61. Power losses decreased dramatically by 63.19%, from 224.76 kW to 82.74 kW, with this final value including SOPs losses. The voltage profile improved, with the minimum voltage rising from 0.90923 p.u. to 0.95445 p.u. Economically, the annual cost of total losses reduced from 224,451.37 to 82,626.54 $/year. Despite additional costs for SOPs investment and maintenance costs of 9712.15 $/year, a substantial net annual saving of 132,112.69 $/year was achieved.

Table 6. IEEE 69-Bus Network Results.

Outputs	Base Case	Optimal Reconfiguration	Optimal Reconfiguration with SOPs Placement
Open switches	69, 70, 71, 72, 73	14, 58, 61, 69, 70	14, 69, 70
Optimal SOP locations (branches)	-	-	56, 61
Optimal SOP sizes: $\{P_{SOP}^{inj,I}(kW), Q_{SOP}^{inj,I}(kVAr), P_{SOP}^{inj,II}(kW), Q_{SOP}^{inj,II}(kVAr)\}$	-	-	SOP_1 {−127.31, 60.45, 124.17, 120.07} SOP_2 {33.53, 259.27, −38.38, 220.16}
Total power loss (kW)	224.76	99.61	82.74
Minimum Voltage (p.u.)	0.90923 (Below limit)	0.94276 (Below limit)	0.95445 (Within limit)
Maximum Voltage (p.u.)	1.00000	1.00000	1.00000
Cost of total loss ($/year)	224,451.37	99,475.61	82,626.54
SOPs investment and maintenance cost ($/year)	-	-	9712.15
Net Saving ($/year)	-	124,975.76	132,112.69

Figure 14 illustrates the voltage profiles for the IEEE 69-bus network under different scenarios. In the base case, voltage levels show a significant drop below the 0.95 p.u. limit, particularly in the remote areas of the network. The reconfiguration with SOPs placement effectively addresses these voltage issues, maintaining all bus voltages above the minimum threshold. This improvement is more pronounced compared to the reconfiguration without SOPs, which shows moderate enhancements but still struggles with voltage regulation in some areas. Figure 15 depicts the topology of the IEEE 69-bus distribution system, showcasing the optimal network configuration and SOPs locations determined by the LF-IEO algorithm.

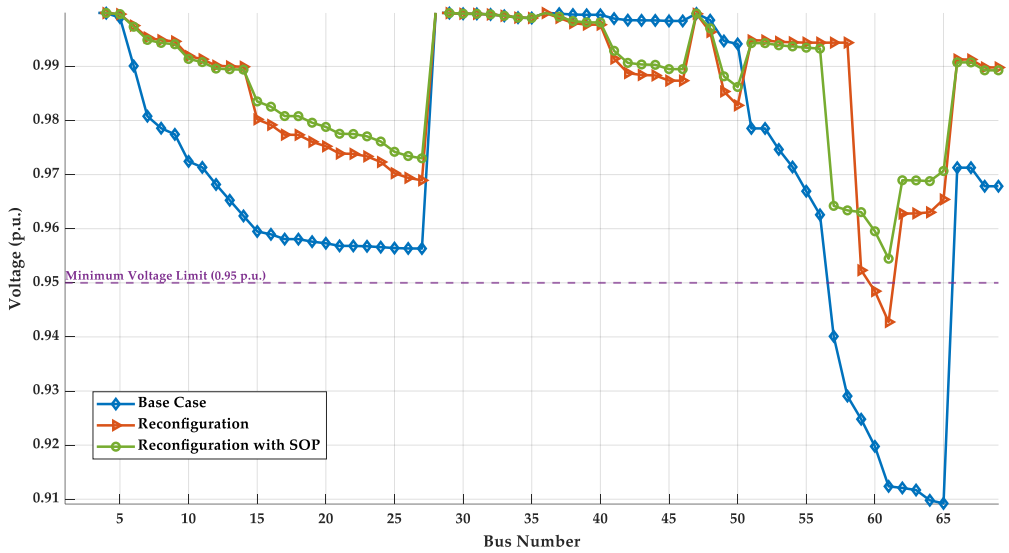

Figure 14. Voltage Profile Comparison for IEEE 69-Bus System.

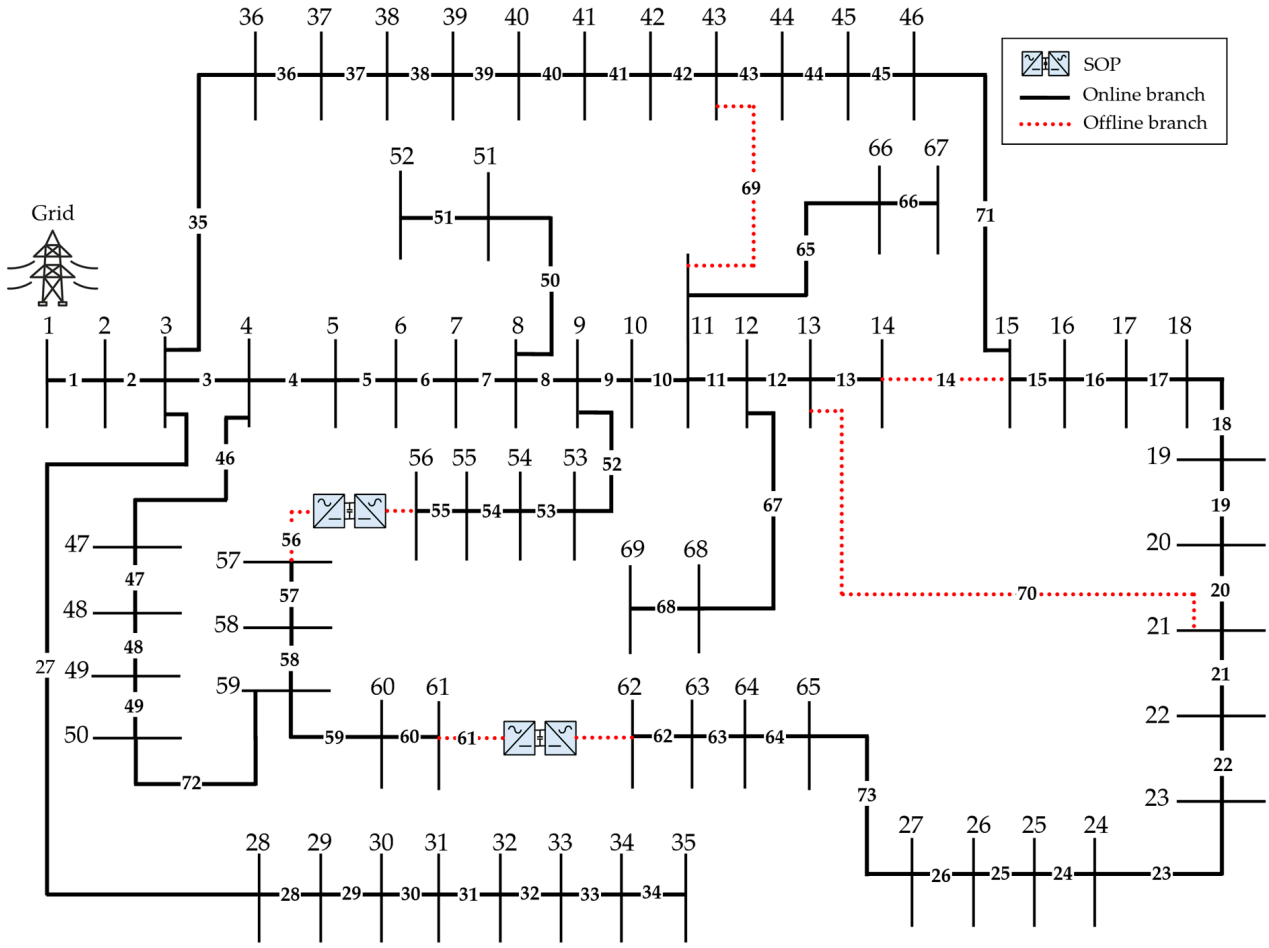

Figure 15. Optimal configuration of the IEEE 69-bus distribution system with SOPs placements.

5.3. IEEE 118-Bus Test System

The IEEE 118-bus system represents a large-scale distribution network that was used to further validate the robustness and scalability of the proposed LF-IEO algorithm. This test system consists of 118 buses and 132 branches, including 117 sectionalizing switches and 15 tie switches. In its initial configuration, switches {118–132} are maintained in open positions. The system operates at a base voltage of 11 kV with a base power of 100 MVA, serving a total load demand of 42.18 MW and 28.14 MVAr. The base case analysis reveals significant operational challenges, with total power losses of 1298.09 kW, translating to an annual cost of 909,698.35 $/year. The voltage profile in the base configuration shows considerable degradation, with the minimum voltage dropping to 0.86880 p.u. at bus 77, well below the acceptable limit of 0.95 p.u., indicating severe voltage regulation issues.

As shown in Table 7, the application of the LF-IEO algorithm for simultaneous optimization of network reconfiguration and SOP placement yielded remarkable improvements. The optimal configuration identified by the algorithm involves new open switch positions at {23, 25, 34, 37, 42, 52, 125, 126, 127, 128, 130} and strategic placement of four SOPs at branches 122, 109, 73, and 95. This configuration achieved a substantial reduction in power losses to 700.34 kW, representing a 46.05% improvement over the base case.

Table 7. IEEE 118-Bus Network Results.

Outputs	Base Case	Optimal Reconfiguration	Optimal Reconfiguration with SOPs Placement
Open switches	118, 119, 120, 121, 122, 123, 124, 125,126, 127, 128, 129, 130, 131, 132	21, 26, 33, 38, 42, 48, 51, 61, 71, 73, 76, 82, 109, 125, 130	23, 25, 34, 37, 42, 52, 58, 70, 76, 82, 130
Optimal SOP locations (branches)	-	-	122, 109, 73, 95
Optimal SOP sizes: $\{P_{SOP}^{inj,I}(kW), Q_{SOP}^{inj,I}(kVAr), P_{SOP}^{inj,II}(kW), Q_{SOP}^{inj,II}(kVAr)\}$	-	-	SOP1 {−368.33, 619.34, 351.19, 929.69} SOP2 {−159.04, 987.22, 139.07, 987.22} SOP3 {−107.17, 333.43, 95.43, 817.61} SOP4 {−221.04, 428.81, 209.28, 661.54}
Total power loss (kW)	1298.09	888.36	700.34
Minimum Voltage (p.u.)	0.86880 (Below limit)	0.93212 (Below limit)	0.95208 (Within limit)
Maximum Voltage (p.u.)	1.00000	1.00000	1.00000
Cost of total loss ($/year)	909,698.35	622,560.21	490,798.85
SOPs investment and maintenance cost ($/year)	-	-	39,394.81
Net Saving ($/year)	-	287,138.14	379,504.69

The voltage profile enhancement is particularly noteworthy, as illustrated in Figure 16. The base case (blue line) shows multiple buses experiencing voltages significantly below the 0.95 p.u. threshold, particularly in the range of buses 65–85. The implementation of optimal reconfiguration with SOPs (green line) successfully raises the minimum voltage to 0.95208 p.u., ensuring all bus voltages remain within acceptable limits. This improvement is more significant than what was achieved through reconfiguration alone (orange line), which still showed some voltage violations.

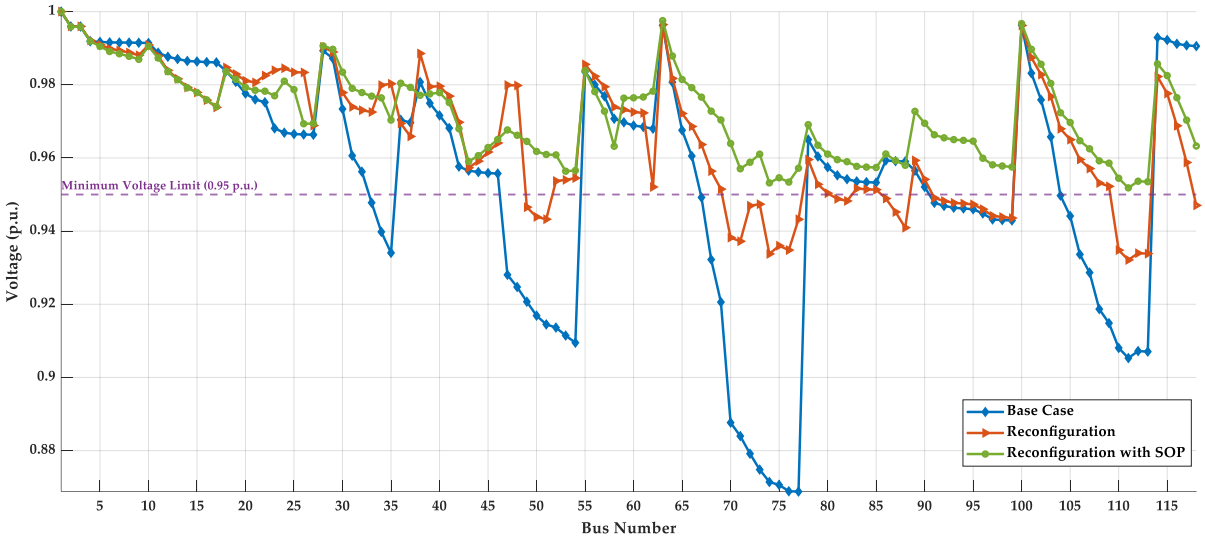

Figure 16. Voltage Profile Comparison for IEEE 118-Bus System.

From an economic perspective, the optimized configuration demonstrates compelling benefits. The reduction in power losses translates to a decrease in annual loss costs from 909,698.35 $/year to 490,798.85 $/year. While the installation and maintenance of four SOPs incurs an annual cost of 39,394.81 $/year, the net annual saving achieved is 379,504.69 $/year, representing a substantial improvement in the system's economic performance. These results further validate the effectiveness of the LF-IEO algorithm in managing large-scale distribution networks while balancing technical and economic objectives. Figure 17 illustrates the topology of the IEEE 118-bus distribution system, showing

the bus connections and the locations of the switches and SOPs in the optimal configuration. The detailed system data and parameters for the IEEE 118-bus system are provided in Appendix B.

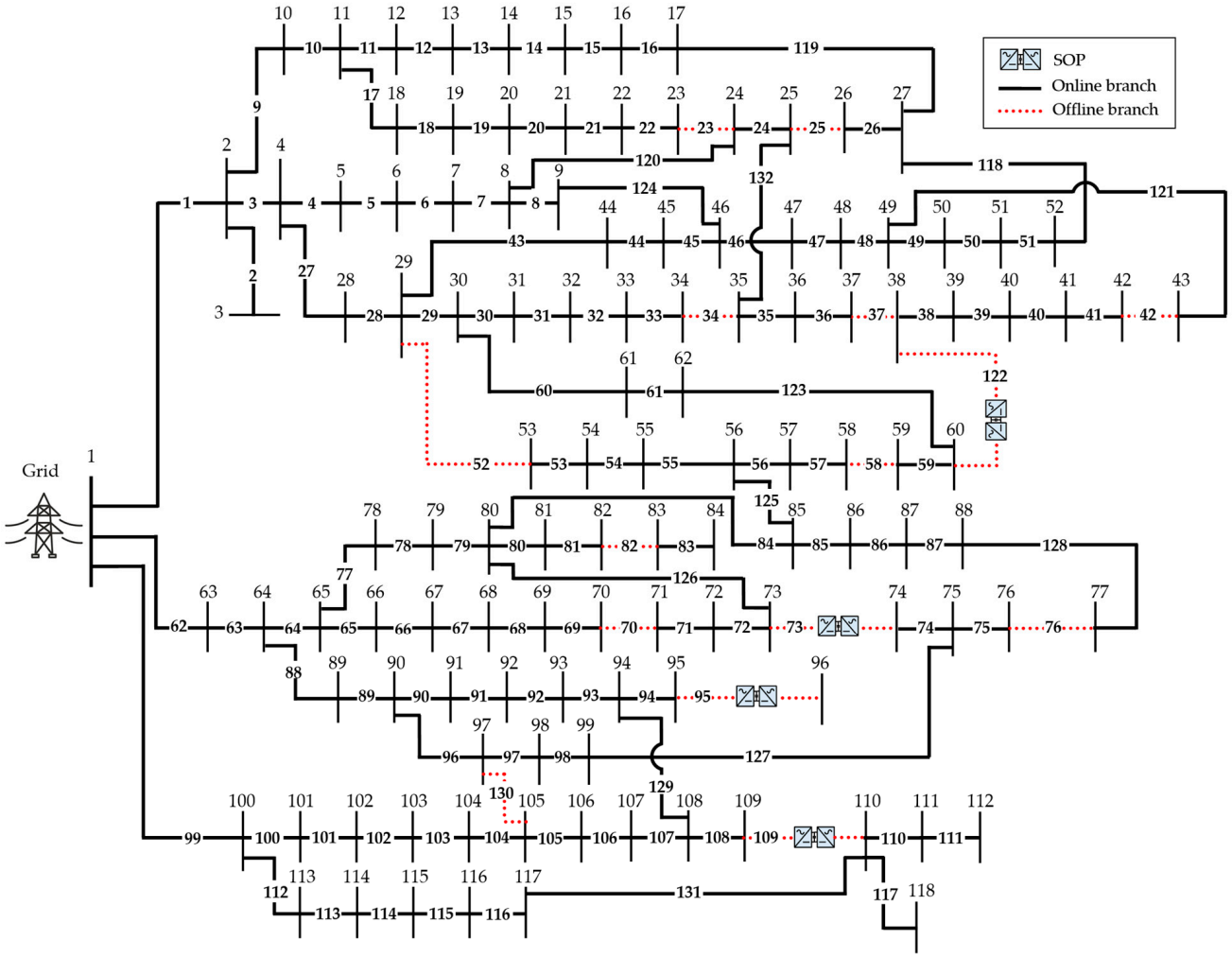

Figure 17. Optimal configuration of the IEEE 118-bus distribution system with SOPs placements.

5.4. Real 116-Bus Distribution System in Algeria

The proposed LF-IEO algorithm was further validated on a real-world 116-bus distribution system from Touggourt City, Algeria. This large-scale network operates at a base voltage of 10 kV with a base power of 100 MVA with a total load of 31.05 MW and 23.29 MVAr. The system comprises 116 buses and 124 branches, including 115 sectionalizing switches and 9 tie switches. In its initial configuration, switches {116, 117, 118, 119, 120, 121, 122, 123, 124} are open. The base case exhibits significant power losses of 687.28 kW, translating to an annual cost of 686,341.77 $/year. The voltage profile ranges from a minimum of 0.96021 p.u. to a maximum of 1.0 p.u.

Application of the LF-IEO algorithm resulted in substantial improvements, as detailed in Table 8. The optimal configuration with SOPs placement reduced power losses by 14.89% to 584.92 kW, with new open switch positions at {21, 28, 41, 65, 99, 123} and three SOPs optimally located at branches 54, 8, and 113. This reconfiguration significantly enhanced the voltage profile, raising the minimum voltage to 0.97108 p.u. The results show that while optimal reconfiguration alone provides some benefits, the addition of SOP placement leads to more significant improvements. The reduction in power loss translates to a decrease in the annual cost of total loss from 686,341.77 $/year to 584,121.17 $/year. Despite a yearly SOPs investment and maintenance cost of 27,794.20 $/year, the optimized system

achieves a notable net annual saving of 74,426.40 $/year, demonstrating the algorithm's effectiveness in improving both technical and economic aspects of this complex, real-world distribution network.

Table 8. Algerian 116-Bus Network Results.

Outputs	Base Case	Optimal Reconfiguration	Optimal Reconfiguration with SOPs Placement
Open switches	116, 117, 118, 119, 120, 121, 122, 123, 124	8, 21, 28, 41, 54, 65, 99, 113, 123	21, 28, 41, 65, 99, 123
Optimal SOP locations (branches)	-	-	54, 8, 113
Optimal SOP sizes: $\{P_{SOP}^{inj,I}(kW), Q_{SOP}^{inj,I}(kVAr), P_{SOP}^{inj,II}(kW), Q_{SOP}^{inj,II}(kVAr)\}$	-	-	SOP_1 {74.02, 238.35, −106.70, 236.74} SOP_2 {12.85, 176.57, 14.57, 176.28} SOP_3 {−19.08, 773.27, 6.88, 773.50}
Total power loss (kW)	687.28	627.86	584.92
Minimum Voltage (p.u.)	0.96021 (Within limit)	0.96628 (Within limit)	0.97108 (Within limit)
Maximum Voltage (p.u.)	1.00000	1.00000	1.00000
Cost of total loss ($/year)	686,341.77	627,003.92	584,121.17
SOPs investment and maintenance cost ($/year)	-	-	27,794.20
Net Saving ($/year)	-	59,337.85	74,426.40

Figure 18 illustrates the voltage profiles for the Algerian 116-bus system under different scenarios. In the base case, while voltage levels are within acceptable limits, there is still room for improvement. The reconfiguration with SOPs placement effectively addresses these voltage issues, maintaining all bus voltages at higher levels and improving the overall voltage profile of the network. This improvement is more pronounced compared to the reconfiguration without SOPs, which shows moderate enhancements but doesn't achieve the same level of voltage regulation across all areas of the network. Figure 19 depicts the topology of the Algerian 116-bus distribution system, showcasing the optimal network configuration and SOPs locations determined by the LF-IEO algorithm.

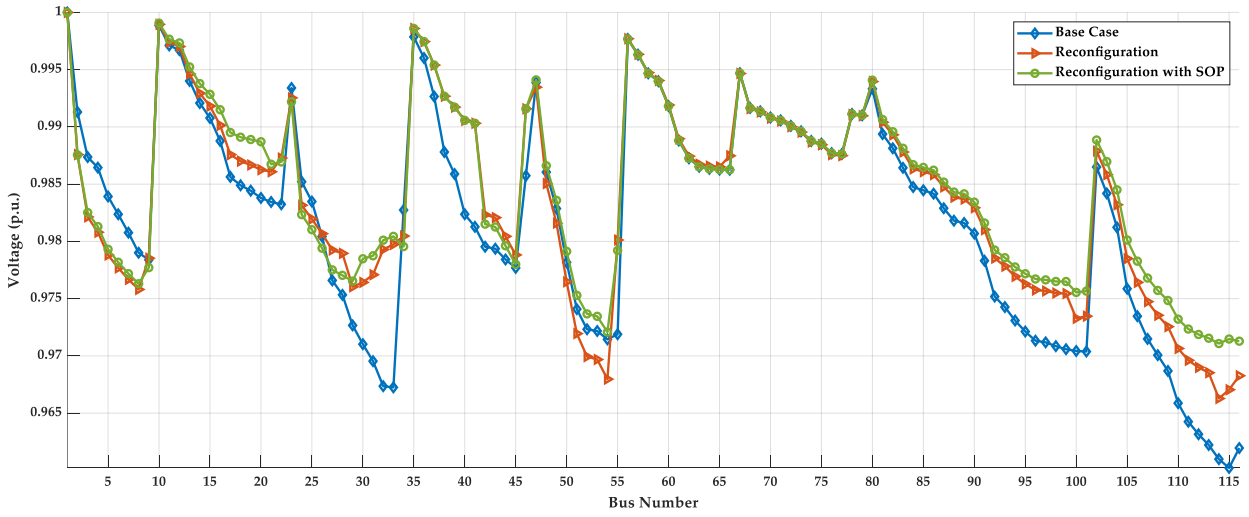

Figure 18. Voltage Profile Comparison for Algerian 116-Bus System.

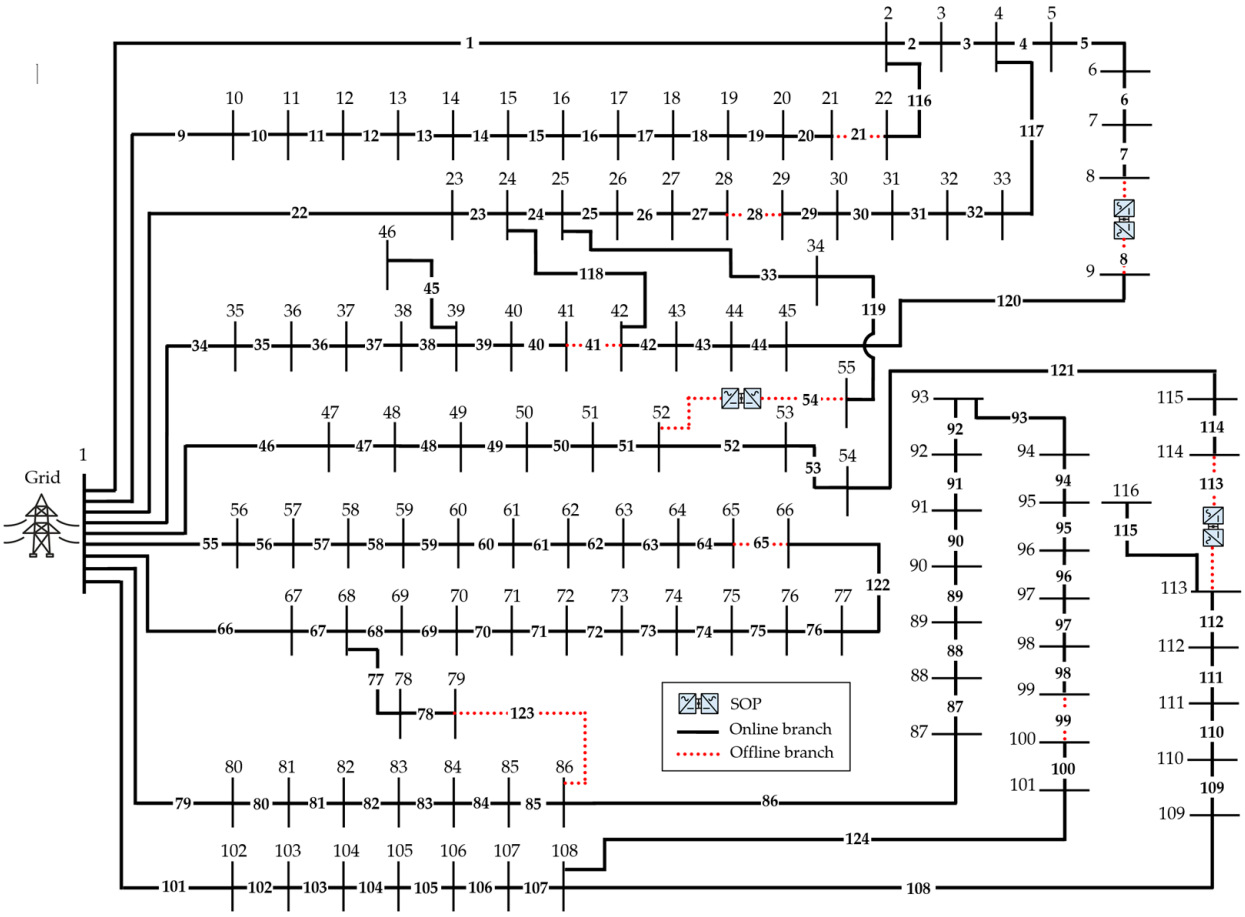

Figure 19. Optimal configuration of the Algerian 116-bus distribution system with SOPs placements.

The application of the LF-IEO algorithm to the Algerian 116-bus system proves its effectiveness in optimizing large-scale, real-world distribution networks. The algorithm successfully reduced power losses, improved voltage profiles, and achieved significant economic benefits, even when accounting for the investment and maintenance costs of the SOPs. This case study, along with the results from the IEEE 33-bus and IEEE 69-bus systems, demonstrates the scalability and robustness of the proposed algorithm across different network sizes and configurations.

Across all tested cases, the optimal SOP parameters obtained through the proposed LF-IEO algorithm have demonstrated a significant impact on the performance of distribution networks. The optimal placement of SOPs, along with their optimal size parameters, enables effective power flow control between feeders. The positive and negative active power parameters facilitate bi-directional power flow, while reactive power parameters ensure localized voltage regulation. This optimal configuration directly reduces power losses and improves voltage profiles. Optimal location of SOPs, coupled with their optimal power parameters, improves load balancing and voltage regulation throughout the feeder, yielding significant annual cost savings. These technical and economic benefits underscore how well-configured SOP parameters enhance the overall performance of distribution networks.

5.5. Comparative Study

The performance of the proposed LF-IEO method for simultaneous reconfiguration and allocation of SOPs in radial distribution systems is illustrated through a comparative study against other algorithms, including GWO, BFO, WOA, MVO, SSA, ALO, and SCA. This comparison, conducted on the Algerian 116-bus system, involved 20 trials for each

methodology, with all techniques aiming to maximize net profit using 1000 iterations and 200 particles.

Table 9 presents a comparative analysis of the algorithms' efficiency indicators, including the best solution achieved, the worst-case scenario, and the standard deviation. The LF-IEO algorithm outperforms the other methods, achieving the highest best solution of 74,426.4 $/year, significantly higher than the next best performer, GWO, at 72,687.6 $/year. The LF-IEO also demonstrates robust performance with the highest worst-case scenario of 67,150.99 $/year and a relatively low standard deviation of 2558.35, indicating consistent high-quality solutions across multiple runs.

Table 9. Comparative Results of Different Optimization Algorithms for the Algerian 116-Bus System.

Alg.	BEST	MEAN	WORST	SD	Best Solution		
					Branches Off	SOPs Branches	SOPs Sizes
GWO	72,687.6	66,046.8	60,354.88	4203.12	20, 41, 54, 65, 98, 123	29, 113, 8	SOP_1 = {11.18, 0.76, −12.30, 99.40}, SOP_2 = {−25.29, 857.37, 8.14, 857.71}, SOP_3 = {2.19, 299.02, −8.17, 298.96}
BFO	48,960.07	28,535.23	12,549.76	13,841.46	8, 30, 41, 63, 98, 114	20, 123, 54	SOP_1 = {−23.59, 62.51, 21.90, 99.42}, SOP_2 = {−20.40, −49.65, 18.80, 104.76}, SOP_3 = {−31.65, 181.20, 28.03, 175.93}
WOA	59,349.94	37,264.18	12,130.4	16,829.43	21, 31, 98, 118, 122, 123	54, 44, 113	SOP_1 = {141.55, 332.04, −148.76, 327.74}, SOP_2 = {−124.13, 332.26, 117.04, 334.73}, SOP_3 = {22.83, 756.52, −37.97, 755.88}
MVO	74,133.66	61,492.54	34,233.77	14,265.32	8, 20, 29, 41, 122, 123	54, 113, 99	SOP_1 = {99.19, 362.10, −106.70, 359.88}, SOP_2 = {−27.23, 632.28, 14.57, 632.69}, SOP_3 = {−11.56, 233.85, 6.88, 233.91}
SSA	63,484.37	44,259.62	14,310.69	18,260.07	7, 20, 41, 64, 99, 123	29, 119, 113	SOP_1 = {28.58, 183.96, −32.30, 183.35}, SOP_2 = {−184.05, 384.71, 175.52, 388.68}, SOP_3 = {−66.09, 750.50, 51.02, 751.68}
ALO	54,762.2	46,404.58	36,867.59	6972.1	21, 28, 41, 54, 65, 123	100, 113, 8	SOP_1 = {−20.55, 248.41, 11.75, 630.81}, SOP_2 = {−76.64, −14.27, 66.67, 916.63}, SOP_3 = {4.85, 267.35, −9.98, 245.59}
SCA	50,260.08	35,863.24	1913.17	17,250.61	30, 41, 65, 116, 120, 123	119, 121, 124	SOP_1 = {23.45, 64.93, −25.39, 122.30}, SOP_2 = {−170.99, 684.04, 156.67, 709.77}, SOP3 = {7.37, 471.35, −16.74, 466.01}
LF-IEO	74,426.4	72,082.52	67,150.99	2558.35	21, 28, 41, 65, 99, 123	54, 8, 113	SOP_1 = {74.02, 238.35, −79.01, 236.74}, SOP_2 = {12.85, 176.57, −16.39, 176.28}, SOP_3 = {−19.08, 773.27, 3.61, 773.50}

The optimal configuration determined by the LF-IEO algorithm involves switching off branches 21, 28, 41, 65, 99, and 123 and placing SOPs at branches 54, 8, and 113. This configuration, along with the specific SOP sizes provided, results in the highest net saving among all tested algorithms. The detailed SOP sizes for LF-IEO are SOP_1 = {74.02, 238.35, −79.01, 236.74}, SOP_2 = {12.85, 176.57, −16.39, 176.28}, and SOP_3 = {−19.08, 773.27, 3.61, 773.50}.

Figure 20 presents box plots comparing the outcomes of various algorithms on both the IEEE 69-bus (a) and Algerian 116-bus (b) systems. These plots provide a visual representation of the distribution of solutions provided by each algorithm across multiple runs. For both systems, the LF-IEO algorithm consistently demonstrates superior performance, with higher median values and smaller interquartile ranges compared to other methods. This is particularly evident in Figure 20b for the larger 116-bus system, where the LF-IEO box is positioned notably higher than the others. The higher position of the LF-IEO boxes in both Figure 20a,b underscores its ability to consistently achieve higher net savings compared to other algorithms, regardless of the system size or complexity. The smaller box size for LF-IEO, especially in Figure 20b, further indicates its more consistent performance across different runs.

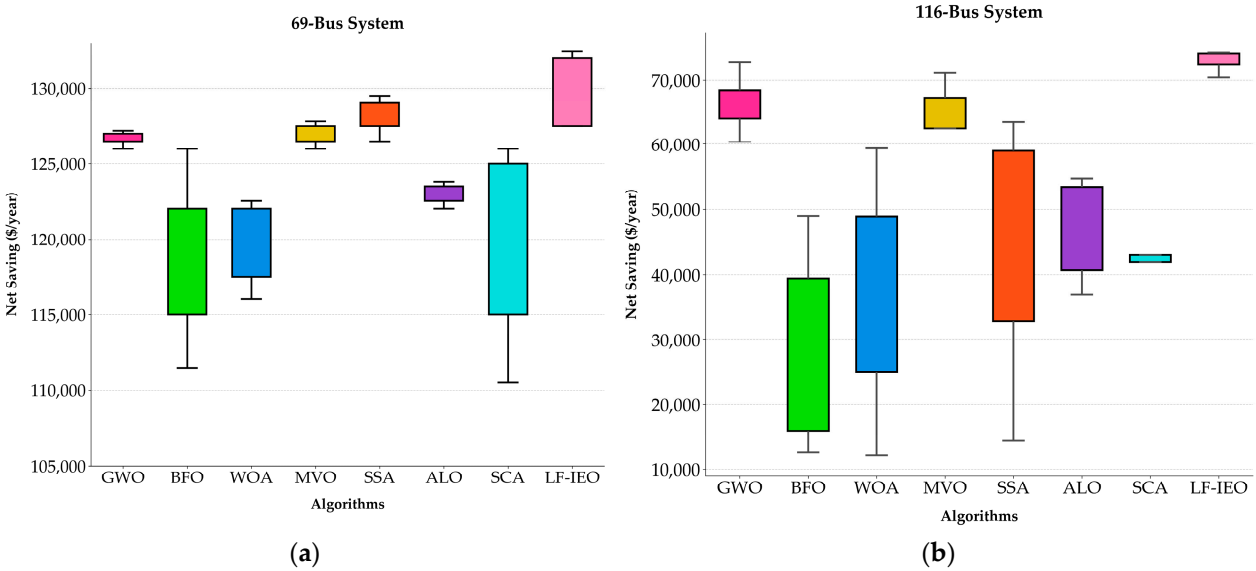

Figure 20. Box Plot Comparison of Net Savings Achieved by Different Algorithms: (**a**) IEEE 69-Bus System; (**b**) Algerian 116-Bus System.

This comprehensive comparison demonstrates that the proposed LF-IEO algorithm not only achieves better results in terms of maximizing net profit but also provides more consistent and reliable solutions across different distribution system sizes [53–55]. Its superior performance in simultaneously optimizing network reconfiguration and SOPs allocation suggests its promising application in improving the efficiency and economical operation of modern distribution networks of varying complexities. The proposed algorithm can be used in other systems as well [56–58].

6. Conclusions

This study introduced a novel Lévy Flight-based Improved Equilibrium Optimizer (LF-IEO) algorithm for the simultaneous optimization of network reconfiguration and Soft Open Points (SOPs) placement in radial distribution systems. To overcome the drawbacks of the traditional Equilibrium Optimizer (EO), the LF-IEO incorporated several key enhancements. These included a Good Point Set (GPS) initialization technique to improve initial population diversity, a Lévy Flight strategy to enhance exploration capabilities, Fast Random Opposition-Based Learning (FROBL) to accelerate convergence, and an oscillating generation probability to maintain a balance of exploration and exploitation. Validation of this optimization technique's effectiveness was achieved through testing on the IEEE 33-bus, IEEE 69-bus, IEEE 118-bus, and a real Algerian 116-bus radial distribution network. The proposed LF-IEO method demonstrated its effectiveness in decreasing active power losses, enhancing the overall voltage quality, and maximizing the net annual savings. Across all test systems, the algorithm achieved significant reductions in power losses, raised minimum voltages above the acceptable threshold, and generated substantial net annual savings. These results underscore the capability of the algorithm to significantly enhance the overall efficiency and reliability of distribution systems while effectively managing the integration of SOPs. Furthermore, the LF-IEO algorithm was evaluated against other widely used optimization techniques, including GWO, BFO, WOA, MVO, SSA, ALO, and SCA. Across multiple runs and different network sizes, the LF-IEO consistently outperformed these methods, demonstrating its robustness and reliability. This superior performance was particularly evident in the large-scale, real-world 116-bus distribution system from Algeria, where the LF-IEO achieved the highest net annual saving, surpassing all other tested algorithms. In conclusion, the LF-IEO algorithm presents a powerful and versatile tool for optimizing radial distribution systems. Its demonstrated ability to simultaneously address network reconfiguration and SOP placement while achieving significant improvements

in system performance makes it a valuable contribution to the field of power system optimization. Further research opportunities include the consideration of data processing under uncertainty environments for network reconfiguration and SOP configuration optimization [59], as well as exploring two-layer optimization approaches to enhance the performance of radial distribution systems [60].

Author Contributions: R.D.M. and M.M. developed the methodology; D.G. and R.D.M. managed software; validation was carried out by M.M., R.D.M. and D.G.; resources were provided by M.M.; R.D.M. handled data curation and prepared the original draft; J.R., M.A. and A.K. reviewed and edited the manuscript; visualization efforts were led by J.R., D.G., M.A. and M.M.; A.K. and A.H. supervised the project. All authors have read and agreed to the published version of the manuscript.

Funding: This research received no external funding.

Data Availability Statement: All data used in this study are provided within the paper and its referenced sources.

Acknowledgments: J. Rodriguez acknowledges the support provided by ANID through projects FB0008, 1210208, and 1221293.

Conflicts of Interest: The authors declare no conflict of interest.

Appendix A

Table A1. List of Abbreviations.

Abbreviation	Definition	Abbreviation	Definition
LF-IEO	Levy Flight	GWO	Grey Wolf Optimizer
EO	Equilibrium Optimizer	BOA	Butterfly Optimization Algorithm
GPS	Good Point Set	WOA	Whale Optimization Algorithm
FROBL	Fast Random Opposition-Based Learning	MVO	Multi-Verse Optimizer
SOP	Soft Open Point	SSA	Salp Swarm Algorithm
BFLF	Backward-Forward Load Flow	ALO	Ant Lion Optimizer
BCBV	Branch Current to Bus Voltage	SCA	Sine Cosine Algorithm
BIBC	Bus Injection to Branch Current	BFO	Bacterial Foraging Optimization
VSC	Voltage Source Converter	NOP	Normally Open Point
OGP	Oscillating Generation Probability	NCC	Normally Closed Condition

Appendix B

Table A2. Bus Data and Branch Data for the IEEE 118-Bus System.

N	Branch		Load at Destination Bus		Branch Parameters			Status
	From	To	P_L (MW)	Q_L (MVAr)	R (p.u.)	X (p.u.)	Imax (A)	
1	1	2	0.133840	0.101140	0.0002975	0.0001074	1200	1
2	2	3	0.016214	0.011292	0.0002727	0.0000983	530	1
3	2	4	0.034315	0.021845	0.0003719	0.0001339	1200	1
4	4	5	0.073016	0.063602	0.0001240	0.0004463	530	1
5	5	6	0.144200	0.068604	0.0001240	0.0004463	530	1
6	6	7	0.104470	0.061725	0.0001240	0.0001033	530	1
7	7	8	0.028547	0.011503	0.0001488	0.0001157	530	1
8	8	9	0.087560	0.051073	0.0001736	0.0005207	530	1
9	2	10	0.198200	0.106770	0.0013719	0.0011107	530	1
10	10	11	0.146800	0.075995	0.0009256	0.0006521	530	1
11	11	12	0.026040	0.018687	0.0015455	0.0025868	530	1
12	12	13	0.052100	0.023220	0.0011736	0.0012496	530	1
13	13	14	0.141900	0.117500	0.0014876	0.0009752	530	1
14	14	15	0.021870	0.028790	0.0012397	0.0003719	530	1
15	15	16	0.033370	0.026450	0.0013223	0.0014876	530	1
16	16	17	0.032430	0.025230	0.0012975	0.0014132	530	1

Table A2. *Cont.*

N	Branch		Load at Destination Bus		Branch Parameters			Status
	From	To	P_L (MW)	Q_L (MVAr)	R (p.u.)	X (p.u.)	Imax (A)	
17	11	18	0.020234	0.011906	0.0018017	0.0023554	530	1
18	18	19	0.156940	0.078523	0.0009752	0.0015289	530	1
19	19	20	0.546290	0.351400	0.0013223	0.0016198	530	1
20	20	21	0.180310	0.164200	0.0009917	0.0015620	530	1
21	21	22	0.093167	0.054594	0.0009917	0.0006521	530	1
22	22	23	0.085180	0.039650	0.0116529	0.0059752	530	1
23	23	24	0.168100	0.095178	0.0024215	0.0011140	530	1
24	24	25	0.125110	0.150220	0.0010992	0.0008595	530	1
25	25	26	0.016030	0.024620	0.0014711	0.0011074	530	1
26	26	27	0.026030	0.024620	0.0014711	0.0011074	530	1
27	4	28	0.594560	0.522620	0.0001240	0.0002446	530	1
28	28	29	0.120620	0.059117	0.0000992	0.0002281	530	1
29	29	30	0.102380	0.099554	0.0009917	0.0022860	530	1
30	30	31	0.513400	0.318500	0.0017355	0.0020083	530	1
31	31	32	0.475250	0.456140	0.0009917	0.0004463	530	1
32	32	33	0.151430	0.136790	0.0014711	0.0019339	530	1
33	33	34	0.205380	0.083302	0.0014711	0.0019339	530	1
34	34	35	0.131600	0.093082	0.0012727	0.0013388	530	1
35	30	36	0.448400	0.369790	0.0015455	0.0021570	530	1
36	36	37	0.440520	0.321640	0.0010992	0.0008182	530	1
37	29	38	0.112540	0.055134	0.0027273	0.0016033	530	1
38	38	39	0.053963	0.038998	0.0025620	0.0016033	530	1
39	39	40	0.393050	0.342600	0.0010744	0.0016033	530	1
40	40	41	0.326740	0.278560	0.0023140	0.0012397	530	1
41	41	42	0.536260	0.240240	0.0097521	0.0070248	530	1
42	42	43	0.076247	0.066562	0.0034711	0.0020132	530	1
43	43	44	0.053520	0.039760	0.0022314	0.0008033	530	1
44	44	45	0.040328	0.031964	0.0028017	0.0010091	530	1
45	45	46	0.039653	0.020758	0.0022314	0.0014702	530	1
46	35	47	0.066195	0.042361	0.0017355	0.0011430	530	1
47	47	48	0.073904	0.051653	0.0009917	0.0006521	530	1
48	48	49	0.114770	0.057965	0.0012397	0.0008157	1200	1
49	49	50	0.918370	1.205100	0.0012397	0.0008157	530	1
50	50	51	0.210300	0.146660	0.0019835	0.0013066	530	1
51	51	52	0.066680	0.056608	0.0009917	0.0006521	530	1
52	52	53	0.042207	0.040184	0.0033471	0.0012050	530	1
53	53	54	0.433740	0.283410	0.0033471	0.0012050	530	1
54	29	55	0.062100	0.026860	0.0032314	0.0011653	530	1
55	55	56	0.092460	0.088380	0.0033554	0.0012074	530	1
56	56	57	0.085188	0.055436	0.0033554	0.0012074	530	1
57	57	58	0.345300	0.332400	0.0058347	0.0045132	530	1
58	58	59	0.022500	0.016830	0.0027934	0.0010066	530	1
59	59	60	0.080551	0.049156	0.0027934	0.0010066	530	1
60	60	61	0.095860	0.090758	0.0017107	0.0006174	530	1
61	61	62	0.062920	0.047700	0.0020413	0.0073736	530	1
62	1	63	0.478800	0.463740	0.0002314	0.0003455	440	1
63	63	64	0.120940	0.052006	0.0009669	0.0016661	440	1
64	64	65	0.139110	0.100340	0.0021074	0.0007587	440	1
65	65	66	0.391780	0.193500	0.0017355	0.0006273	530	1
66	66	67	0.027741	0.026713	0.0031653	0.0011405	530	1
67	67	68	0.052814	0.025257	0.0041653	0.0027298	530	1
68	68	69	0.066890	0.038713	0.0033554	0.0012074	530	1
69	69	70	0.467500	0.395140	0.0079504	0.0062893	530	1
70	70	71	0.594850	0.239740	0.0013636	0.0004959	530	1
71	71	72	0.132500	0.084363	0.0025041	0.0009025	530	1
72	72	73	0.052699	0.022482	0.0025041	0.0009025	530	1
73	73	74	0.869790	0.614775	0.0017025	0.0011901	440	1
74	74	75	0.031349	0.029817	0.0019256	0.0006942	530	1
75	75	76	0.192390	0.122430	0.0048843	0.0014653	530	1
76	76	77	0.065750	0.045370	0.0010413	0.0003744	530	1
77	64	78	0.238150	0.223220	0.0046198	0.0030471	530	1
78	78	79	0.294550	0.162470	0.0015372	0.0010140	530	1
79	79	80	0.485570	0.437920	0.0015372	0.0010140	530	1
80	80	81	0.243530	0.183030	0.0021488	0.0011488	530	1
81	81	82	0.243530	0.183030	0.0012727	0.0012231	530	1
82	82	83	0.134250	0.119290	0.0019008	0.0010579	440	1
83	83	84	0.022710	0.027960	0.0020826	0.0008760	530	1

Table A2. *Cont.*

N	Branch		Load at Destination Bus		Branch Parameters			Status
	From	To	P_L (MW)	Q_L (MVAr)	R (p.u.)	X (p.u.)	Imax (A)	
84	84	85	0.049513	0.026515	0.0014876	0.0012231	530	1
85	79	86	0.383780	0.257160	0.0013223	0.0015041	530	1
86	86	87	0.049640	0.020600	0.0016529	0.0019008	530	1
87	87	88	0.022473	0.011806	0.0013223	0.0032479	530	1
88	65	89	0.062930	0.042960	0.0055289	0.0019934	530	1
89	89	90	0.030670	0.034930	0.0021983	0.0010140	530	1
90	90	91	0.062530	0.066790	0.0021983	0.0010140	530	1
91	91	92	0.114570	0.081748	0.0021983	0.0010140	530	1
92	92	93	0.081292	0.066526	0.0021983	0.0010140	530	1
93	93	94	0.031733	0.015960	0.0019256	0.0009504	530	1
94	94	95	0.033320	0.060480	0.0040992	0.0011405	530	1
95	91	96	0.531280	0.224850	0.0016198	0.0014876	530	1
96	96	97	0.507030	0.367420	0.0016198	0.0014876	530	1
97	97	98	0.026390	0.011700	0.0015421	0.0010083	530	1
98	98	99	0.045990	0.030392	0.0006165	0.0026281	530	1
99	1	100	0.100660	0.047572	0.0005165	0.0002190	530	1
100	100	101	0.456480	0.350300	0.0012405	0.0019339	530	1
101	101	102	0.522560	0.449290	0.0011132	0.0007339	530	1
102	102	103	0.408430	0.168460	0.0019066	0.0009942	530	1
103	103	104	0.141480	0.134250	0.0036942	0.0013289	530	1
104	104	105	0.104430	0.066024	0.0013488	0.0004860	530	1
105	105	106	0.096793	0.083647	0.0027273	0.0008182	530	1
106	106	107	0.493920	0.419340	0.0012893	0.0004636	530	1
107	107	108	0.225380	0.135880	0.0031562	0.0011355	530	1
108	108	109	0.509210	0.387210	0.0013438	0.0004835	530	1
109	109	110	0.188500	0.173460	0.0031562	0.0011355	530	1
110	110	111	0.918030	0.898550	0.0020207	0.0007264	530	1
111	110	112	0.305080	0.215370	0.0017256	0.0006223	530	1
112	112	113	0.054380	0.040970	0.0019017	0.0006843	530	1
113	100	114	0.211140	0.192900	0.0050430	0.0018149	530	1
114	114	115	0.067009	0.053336	0.0015421	0.0010496	530	1
115	115	116	0.162070	0.090321	0.0030843	0.0020331	530	1
116	116	117	0.048785	0.029156	0.0033471	0.0030331	530	1
117	117	118	0.033900	0.018980	0.0040413	0.0036198	530	1
118	46	27	-	-	0.0043455	0.0024174	530	0
119	17	27	-	-	0.0043455	0.0024099	530	0
120	8	24	-	-	0.0035306	0.0012719	530	0
121	54	43	-	-	0.0039669	0.0014281	530	0
122	62	49	-	-	0.0029752	0.0010711	530	0
123	37	62	-	-	0.0047107	0.0047273	530	0
124	9	40	-	-	0.0043802	0.0027669	530	0
125	58	96	-	-	0.0032702	0.0011777	530	0
126	73	91	-	-	0.0056198	0.0053554	530	0
127	88	75	-	-	0.0033570	0.0012099	530	0
128	99	77	-	-	0.0038231	0.0013835	530	0
129	108	83	-	-	0.0053802	0.0019339	530	0
130	105	86	-	-	0.0067149	0.0024174	530	0
131	110	118	-	-	0.0058587	0.0021099	530	0
132	25	35	-	-	0.0041322	0.0041322	530	0

References

1. Shahnia, F.; Arefi, A.; Ledwich, G. *Electric Distribution Network Planning*; Springer: Berlin/Heidelberg, Germany, 2018; Volume 400.
2. Mahdavi, M.; Alhelou, H.H.; Hatziargyriou, N.D.; Jurado, F. Reconfiguration of electric power distribution systems: Comprehensive review and classification. *IEEE Access* **2021**, *9*, 118502–118527. [CrossRef]
3. Saaklayen, M.A.; Liang, X.; Faried, S.O.; Mitolo, M. Soft Open Points in Active Distribution Systems. In *Smart and Power Grid Systems—Design Challenges and Paradigms*; River Publishers: Gistrup, Denmark, 2023; pp. 253–285.
4. Azizi, A.; Vahidi, B.; Nematollahi, A.F. Reconfiguration of active distribution networks equipped with soft open points considering protection constraints. *J. Mod. Power Syst. Clean Energy* **2023**, *11*, 212–222. [CrossRef]
5. Janamala, V.; Radha Rani, K.; Sobha Rani, P.; Venkateswarlu, A.; Inkollu, S.R. Optimal switching operations of soft open points in active distribution network for handling variable penetration of photovoltaic and electric vehicles using artificial rabbits optimization. *Process Integr. Optim. Sustain.* **2023**, *7*, 419–437. [CrossRef]

6. Sreenivasulu Reddy, D.; Janamala, V. Political Optimizer-Based Optimal Integration of Soft Open Points and Renewable Sources for Improving Resilience in Radial Distribution System. In Proceedings of the Congress on Intelligent Systems: Proceedings of CIS 2021; Springer: Singapore, 2022; Volume 1, pp. 439–449.
7. Li, L.; Yu, H.; Liu, Y.; Liu, W.; Huang, M.; Zhang, P.; You, X.; Li, S. Optimal control method of active distribution network considering soft open point and thermostatically controlled loads under distributed photovoltaic access. *Syst. Sci. Control. Eng.* **2023**, *11*, 2228334. [CrossRef]
8. Chen, Z.; He, Y.; Hua, Y.; Wu, H.; Bi, R. Coordinated planning of DGs and soft open points in multi-voltage level distributed networks based on the Stackelberg game. *IET Renew. Power Gener.* **2024**, *18*, 2942–2955. [CrossRef]
9. Pamshetti, V.B.; Singh, S.; Singh, S.P. Reduction of energy demand via conservation voltage reduction considering network reconfiguration and soft open point. *Int. Trans. Electr. Energy Syst.* **2020**, *30*, e12147. [CrossRef]
10. Liu, G.; Sun, W.; Hong, H.; Shi, G. Coordinated Configuration of SOPs and DESSs in an Active Distribution Network Considering Social Welfare Maximization. *Sustainability* **2024**, *16*, 2247. [CrossRef]
11. Ebrahimi, H.; Galvani, S.; Talavat, V.; Farhadi-Kangarlu, M. A conditional value at risk based stochastic allocation of SOP in distribution networks. *Electr. Power Syst. Res.* **2024**, *228*, 110111. [CrossRef]
12. Rezaeian-Marjani, S.; Galvani, S.; Talavat, V. A generalized probabilistic multi-objective method for optimal allocation of soft open point (SOP) in distribution networks. *IET Renew. Power Gener.* **2022**, *16*, 1046–1072. [CrossRef]
13. Farzamnia, A.; Marjani, S.; Galvani, S.; Kin, K.T.T. Optimal allocation of soft open point devices in renewable energy integrated distribution systems. *IEEE Access* **2022**, *10*, 9309–9320. [CrossRef]
14. Linh, N.T.; Long, P.V. Optimizing the Location and Capacity of DGs and SOPs in Distribution Networks using an Improved Artificial Bee Colony Algorithm. *Eng. Technol. Appl. Sci. Res.* **2024**, *14*, 15171–15179. [CrossRef]
15. Nguyen, T.T.; Nguyen, T.T.; Nguyen, H.P. Optimal soft open point placement and open switch position selection simultaneously for power loss reduction on the electric distribution network. *Expert Syst. Appl.* **2024**, *238*, 121743. [CrossRef]
16. Gholami, K.; Azizivahed, A.; Arefi, A.; Arif, M.T.; Haque, M.E. Simultaneous allocation of soft open points and tie switches in harmonic polluted distribution networks. *Electr. Power Syst. Res.* **2024**, *234*, 110568. [CrossRef]
17. Wang, K.; Xue, Y.; Zhou, Y.; Li, Z.; Chang, X.; Sun, H. Distributed coordinated reconfiguration with soft open points for resilience-oriented restoration in integrated electric and heating systems. *Appl. Energy* **2024**, *365*, 123207. [CrossRef]
18. Diaaeldin, I.; Abdel Aleem, S.; El-Rafei, A.; Abdelaziz, A.; Zobaa, A.F. Optimal network reconfiguration in active distribution networks with soft open points and distributed generation. *Energies* **2019**, *12*, 4172. [CrossRef]
19. Cao, W.; Wu, J.; Jenkins, N.; Wang, C.; Green, T. Benefits analysis of soft open points for electrical distribution network operation. *Appl. Energy* **2016**, *165*, 36–47. [CrossRef]
20. Van Tran, H.; Truong, A.V.; Phan, T.M.; Nguyen, T.T. Optimal placement and operation of soft open points, capacitors, and renewable distributed generators in distribution power networks to reduce total one-year energy loss. *Heliyon* **2024**, *10*, e26845. [CrossRef]
21. Faramarzi, A.; Heidarinejad, M.; Stephens, B.; Mirjalili, S. Equilibrium optimizer: A novel optimization algorithm. *Knowl.-Based Syst.* **2020**, *191*, 105190. [CrossRef]
22. Mansour, S.; Badr, A.O.; Attia, M.A.; Sameh, M.A.; Kotb, H.; Elgamli, E.; Shouran, M. Fuzzy Logic Controller Equilibrium Base to Enhance AGC System Performance with Renewable Energy Disturbances. *Energies* **2022**, *15*, 6709. [CrossRef]
23. Zellagui, M.; Belbachir, N.; Lasmari, A.; Molu, R.J.J.; Kamel, S. Enhancing PV distributed generator planning in medium-voltage DC distribution networks: A multi-design techno-economic analysis with load demand response. *IET Gener. Transm. Distrib.* **2024**, *18*, 173–189. [CrossRef]
24. Djamel, M.R.; Mustafa, M.; Rabie, Z.; Abdelouahab, K.; Sidi, M.O.; Soufi, Y. A Novel Equilibrium Optimization Algorithm for Optimal Coordination of Directional Overcurrent Relays. In Proceedings of the 2023 International Conference on Electrical Engineering and Advanced Technology (ICEEAT), Batna, Algeria, 5–7 November 2023; pp. 1–6.
25. Korashy, A.; Kamel, S.; Jurado, F.; Fendzi Mbasso, W. OptiCoord: Advancing directional overcurrent and distance relay coordination with an enhanced equilibrium optimizer. *Heliyon* **2024**, *10*, e26366. [CrossRef] [PubMed]
26. Dao, T.M.; Huy, T.H.B.; Do, D.-P.N.; Ngoc Vo, D. A chaotic equilibrium optimization for temperature-dependent optimal power flow. *Smart Sci.* **2023**, *11*, 380–394. [CrossRef]
27. Chankaya, M.; Naqvi, S.B.Q.; Hussain, I.; Singh, B.; Ahmad, A. Power quality enhancement and improved dynamics of a grid tied PV system using equilibrium optimization control based regulation of DC bus voltage. *Electr. Power Syst. Res.* **2024**, *226*, 109911. [CrossRef]
28. Jiang, R.; Wang, X.; Cao, S.; Zhao, J.; Li, X. Joint compressed sensing and enhanced whale optimization algorithm for pilot allocation in underwater acoustic OFDM systems. *IEEE Access* **2019**, *7*, 95779–95796. [CrossRef]
29. Li, J.; An, Q.; Lei, H.; Deng, Q.; Wang, G.-G. Survey of Lévy Flight-Based Metaheuristics for Optimization. *Mathematics* **2022**, *10*, 2785. [CrossRef]
30. Mohapatra, S.; Mohapatra, P. Fast random opposition-based learning Golden Jackal Optimization algorithm. *Knowl.-Based Syst.* **2023**, *275*, 110679. [CrossRef]
31. Mirjalili, S.; Mirjalili, S.M.; Lewis, A. Grey Wolf Optimizer. *Adv. Eng. Softw.* **2014**, *69*, 46–61. [CrossRef]
32. Arora, S.; Singh, S. Butterfly optimization algorithm: A novel approach for global optimization. *Soft Comput.* **2019**, *23*, 715–734. [CrossRef]

33. Mirjalili, S.; Lewis, A. The Whale Optimization Algorithm. *Adv. Eng. Softw.* **2016**, *95*, 51–67. [CrossRef]
34. Mirjalili, S.; Mirjalili, S.M.; Hatamlou, A. Multi-Verse Optimizer: A nature-inspired algorithm for global optimization. *Neural Comput. Appl.* **2016**, *27*, 495–513. [CrossRef]
35. Mirjalili, S.; Gandomi, A.H.; Mirjalili, S.Z.; Saremi, S.; Faris, H.; Mirjalili, S.M. Salp Swarm Algorithm: A bio-inspired optimizer for engineering design problems. *Adv. Eng. Softw.* **2017**, *114*, 163–191. [CrossRef]
36. Mirjalili, S. The Ant Lion Optimizer. *Adv. Eng. Softw.* **2015**, *83*, 80–98. [CrossRef]
37. Mirjalili, S. SCA: A Sine Cosine Algorithm for solving optimization problems. *Knowl.-Based Syst.* **2016**, *96*, 120–133. [CrossRef]
38. Bloemink, J.M.; Green, T.C. Increasing photovoltaic penetration with local energy storage and soft normally-open points. In Proceedings of the 2011 IEEE Power and Energy Society General Meeting, Detroit, MI, USA, 24–29 July 2011; pp. 1–8.
39. Ehsanbakhsh, M.; Sepasian, M.S. Simultaneous siting and sizing of Soft Open Points and the allocation of tie switches in active distribution network considering network reconfiguration. *IET Gener. Transm. Distrib.* **2023**, *17*, 263–280. [CrossRef]
40. Rahimipour Behbahani, M.; Jalilian, A. Optimal operation of soft open point devices and distribution network reconfiguration in a harmonically polluted distribution network. *Electr. Power Syst. Res.* **2024**, *237*, 110967. [CrossRef]
41. Wang, C.; Song, G.; Li, P.; Ji, H.; Zhao, J.; Wu, J. Optimal siting and sizing of soft open points in active electrical distribution networks. *Appl. Energy* **2017**, *189*, 301–309. [CrossRef]
42. Wang, X.; Guo, Q.; Tu, C.; Li, J.; Xiao, F.; Wan, D. A two-stage optimal strategy for flexible interconnection distribution network considering the loss characteristic of key equipment. *Int. J. Electr. Power Energy Syst.* **2023**, *152*, 109232. [CrossRef]
43. Yang, L.; Li, Y.; Zhang, Y.; Xie, Z.; Chen, J.; Qu, Y. Optimal allocation strategy of SOP in flexible interconnected distribution network oriented high proportion renewable energy distribution generation. *Energy Rep.* **2024**, *11*, 6048–6056. [CrossRef]
44. Kawambwa, S.; Mwifunyi, R.; Mnyanghwalo, D.; Hamisi, N.; Kalinga, E.; Mvungi, N. An improved backward/forward sweep power flow method based on network tree depth for radial distribution systems. *J. Electr. Syst. Inf. Technol.* **2021**, *8*, 7. [CrossRef]
45. Ali, A.; Keerio, M.U.; Laghari, J.A. Optimal Site and Size of Distributed Generation Allocation in Radial Distribution Network Using Multi-objective Optimization. *J. Mod. Power Syst. Clean Energy* **2021**, *9*, 404–415. [CrossRef]
46. Rahimi, I.; Gandomi, A.H.; Chen, F.; Mezura-Montes, E. A Review on Constraint Handling Techniques for Population-based Algorithms: From single-objective to multi-objective optimization. *Arch. Comput. Methods Eng.* **2023**, *30*, 2181–2209. [CrossRef]
47. Roberge, V.; Tarbouchi, M.; Okou, F.A. Distribution system optimization on graphics processing unit. *IEEE Trans. Smart Grid* **2015**, *8*, 1689–1699. [CrossRef]
48. Diestel, R. *Graph Theory*; Springer: Berlin/Heidelberg, Germany, 2024.
49. Yang, W.Y.; Cao, W.; Kim, J.; Park, K.W.; Park, H.-H.; Joung, J.; Ro, J.-S.; Lee, H.L.; Hong, C.-H.; Im, T. *Applied Numerical Methods Using MATLAB*; John Wiley & Sons: Hoboken, NJ, USA, 2020.
50. Ghasemi, S. Balanced and unbalanced distribution networks reconfiguration considering reliability indices. *Ain Shams Eng. J.* **2018**, *9*, 1567–1579. [CrossRef]
51. Nguyen, T.T.; Nguyen, T.T. An improved cuckoo search algorithm for the problem of electric distribution network reconfiguration. *Appl. Soft Comput.* **2019**, *84*, 105720. [CrossRef]
52. Savier, J.; Das, D. Impact of network reconfiguration on loss allocation of radial distribution systems. *IEEE Trans. Power Deliv.* **2007**, *22*, 2473–2480. [CrossRef]
53. Shirkhani, M.; Tavoosi, J.; Danyali, S.; Sarvenoee, A.K.; Abdali, A.; Mohammadzadeh, A.; Zhang, C. A review on microgrid decentralized energy/voltage control structures and methods. *Energy Rep.* **2023**, *10*, 368–380. [CrossRef]
54. Meng, Q.; Tong, X.; Hussain, S.; Luo, F.; Zhou, F.; He, Y.; Li, B. Enhancing distribution system stability and efficiency through multi-power supply startup optimization for new energy integration. *IET Gener. Transm. Distrib.* **2024**, *18*, 3487–3500. [CrossRef]
55. Duan, Y.; Zhao, Y.; Hu, J. An initialization-free distributed algorithm for dynamic economic dispatch problems in microgrid: Modeling, optimization and analysis. *Sustain. Energy Grids Netw.* **2023**, *34*, 101004. [CrossRef]
56. Ma, K.; Yang, J.; Liu, P. Relaying-Assisted Communications for Demand Response in Smart Grid: Cost Modeling, Game Strategies, and Algorithms. *IEEE J. Sel. Areas Commun.* **2020**, *38*, 48–60. [CrossRef]
57. Zhang, J.; Feng, X.; Zhou, J.; Zang, J.; Wang, J.; Shi, G.; Li, Y. Series-Shunt Multiport Soft Normally Open Points. *IEEE Trans. Ind. Electron.* **2023**, *70*, 10811–10821. [CrossRef]
58. Zhang, J.; Li, H.; Kong, X.; Zhou, J.; Shi, G.; Zang, J.; Wang, J. A Novel Multiple-Medium-AC-Port Power Electronic Transformer. *IEEE Trans. Ind. Electron.* **2024**, *71*, 6568–6578. [CrossRef]
59. Ding, B.; Li, Z.; Li, Z.; Xue, Y.; Chang, X.; Su, J.; Jin, X.; Sun, H. A CCP-based distributed cooperative operation strategy for multi-agent energy systems integrated with wind, solar, and buildings. *Appl. Energy* **2024**, *365*, 123275. [CrossRef]
60. Zhang, H.; Li, Z.; Xue, Y.; Chang, X.; Su, J.; Wang, P.; Guo, Q.; Sun, H. A Stochastic Bi-level Optimal Allocation Approach of Intelligent Buildings Considering Energy Storage Sharing Services. *IEEE Trans. Consum. Electron.* **2024**, 1. [CrossRef]